HHS Public Access

Author manuscript

Cell Rep. Author manuscript; available in PMC 2023 December 18.

Published in final edited form as:

Cell Rep. 2023 November 28; 42(11): 113329. doi:10.1016/j.celrep.2023.113329.

PRMT5 mediates FoxO1 methylation and subcellular localization to regulate lipophagy in myogenic progenitors

Kun Ho Kim[1], **Stephanie N. Oprescu**[1,2], **Madigan M. Snyder**[1,2], **Aran Kim**[3], **Zhihao Jia**[1,5], **Feng Yue**[1,6], **Shihuan Kuang**[1,4,7,*]

[1]Department of Animal Sciences, Purdue University, West Lafayette, IN 47907, USA

[2]Department of Biological Sciences, Purdue University, West Lafayette, IN 47907, USA

[3]Department of Pharmacy, Purdue University, West Lafayette, IN 47907, USA

[4]Center for Cancer Research, Purdue University, West Lafayette, IN 47907, USA

[5]Present address: Cambridge-Suda Genomic Resource Center, Suzhou Medical College, Soochow University, Suzhou, China

[6]Present address: Department of Animal Sciences, University of Florida, Gainesville, FL 32611, USA

[7]Lead contact

SUMMARY

Development is regulated by various factors, including protein methylation status. While PRMT5 is well known for its roles in oncogenesis by mediating symmetric di-methylation of arginine, its role in normal development remains elusive. Using *Myod1*^{Cre} to drive *Prmt5* knockout in embryonic myoblasts (*Prmt5*^{MKO}), we dissected the role of PRMT5 in myogenesis. The *Prmt5*^{MKO} mice are born normally but exhibit progressive muscle atrophy and premature death. *Prmt5*^{MKO} inhibits proliferation and promotes premature differentiation of embryonic myoblasts, reducing the number and regenerative function of satellite cells in postnatal mice. Mechanistically, PRMT5 methylates and destabilizes FoxO1. *Prmt5*^{MKO} increases the total FoxO1 level and promotes its cytoplasmic accumulation, leading to activation of autophagy and depletion of lipid droplets (LDs). Systemic inhibition of autophagy in *Prmt5*^{MKO} mice restores LDs in myoblasts and moderately improves muscle regeneration. Together, PRMT5 is essential for muscle development and regeneration at least partially through mediating FoxO1 methylation and LD turnover.

*Correspondence: skuang@purdue.edu.

AUTHOR CONTRIBUTIONS

K.H.K. and S.K. conceived the project and designed the experiments. K.H.K., S.O., M.S., A.K., Z.J., and F.Y. performed *in vitro* and *in vivo* experiments and analyzed the data. K.H.K. and S.K. wrote the manuscript and integrated comments for the other authors.

DECLARATION OF INTERESTS

The authors declare no competing interests.

SUPPLEMENTAL INFORMATION

Supplemental information can be found online at https://doi.org/10.1016/j.celrep.2023.113329.

In brief

Kim et al. report the role of PRMT5 in muscle development using knockout (KO) mice. Myoblast-specific *Prmt5*-KO impairs myogenesis and causes premature death. PRMT5 regulates subcellular localization of FoxO1, which influences autophagy of lipid droplets. The work uncovers an interplay between PRMT5, FoxO1, and lipophagy essential for muscle development.

Graphical Abstract

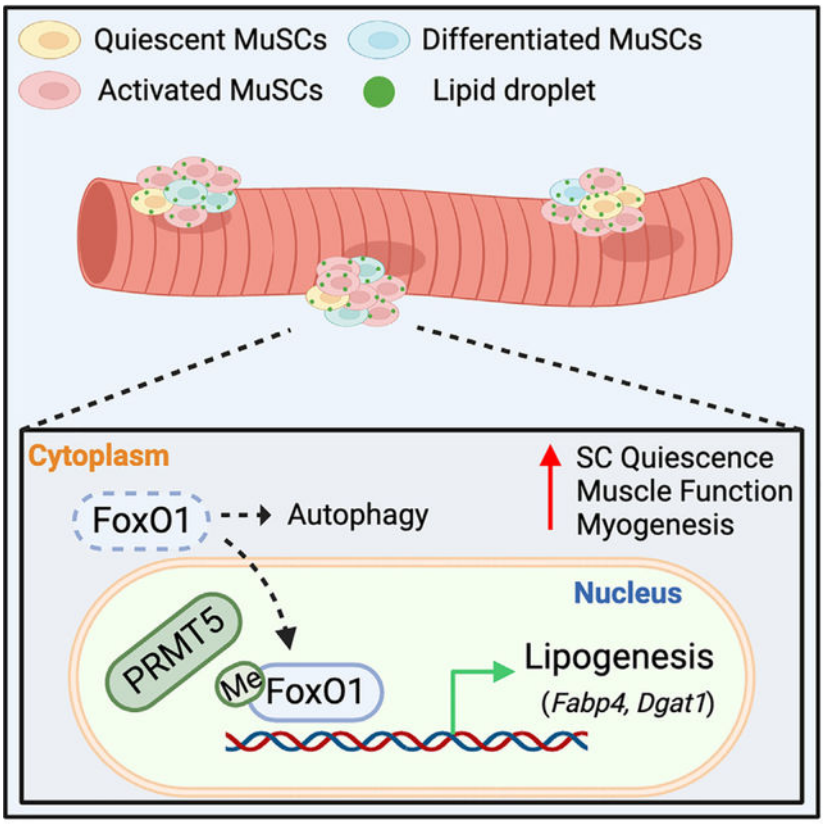

INTRODUCTION

Embryonic myogenic progenitor cells (also called myoblasts) and adult satellite cells (SCs) play an essential role in muscle development and regeneration, respectively.[1,2] Embryonic and fetal myogenesis involves two stages of muscle fiber (myofiber) formation.[3,4] The first phase, referred to as primary myogenesis, takes place at embryonic day (E) 9.5–14.5, encompassing the differentiation of myoblasts into primary myofibers.[3,4] Subsequently, secondary myogenesis occurs at E14.5–17.5, during which myoblasts continue to proliferate and differentiate to form secondary myofibers, as well as deposit SCs at the peripheral of myofibers.[3,4] These secondary myofibers are composed of a heterogeneous cell population with different contractile, physiological, and biochemical properties, thereby contributing to the overall morphogenesis and function of a complex musculature.[3,4] In the neonatal mice, SCs account for up to 30% of muscle nuclei and undergo extensive proliferation to contribute nuclei to growing myofibers.[5] This process of myonuclear accretion through SC

proliferation and fusion is crucial for postnatal muscle growth. SCs become quiescent in adult, but they can be activated by muscle injury or other cues to rapidly proliferate and differentiate to repair the injured muscles. Together, proliferation of myoblasts and SCs is critical for muscle development, growth, and regeneration.

Macroautophagy (hereafter referred to as autophagy) serves as an intracellular adaptive mechanism, sustaining quality control and recycling of misfolded proteins and dysfunctional organelles under normal and stress conditions.[6] Substantial evidence suggests that proper autophagic activity is necessary for myoblast proliferation, muscle development, and regeneration, as it regulates protein turnover and provides the essential components and energy for new protein synthesis.[7–10] Autophagy is triggered to provide bioenergetic support when quiescent SCs become activated, but excessive autophagy activation has been implicated in a plethora of muscular diseases, including muscle atrophy and degeneration.[6,11–13] Accumulating evidence has demonstrated that autophagy is indispensable for the breakdown of lipid droplets (LDs) (a process called lipophagy) in skeletal muscle tissues, and the dynamic turnover of LDs is vital in determining the fate of SCs.[14,15] Despite considerable understanding on the regulation of LD degradation through autophagic flux, including lipophagy,[15] the molecular mechanisms regulating lipophagy in SCs remain poorly characterized.

FoxO1, a member of the FoxO protein family, primarily functions as a transcription factor that regulates gene expression. In this regard, we have shown that nuclear FoxO1 interacts with Notch Intracellular Domain (NICD) to enforce SC quiescence.[16] In addition, FoxO1 has also been reported to regulate various physiological processes (such as autophagy) beyond its nuclear functions.[17] Accumulating evidence has demonstrated that cytosolic FoxO1, regulated by post-translational modifications (PTMs), triggers autophagy.[18,19] Specifically, acetylation of FoxO1 promotes its binding to ATG7, the autophagic initiation protein, thereby stimulating autophagy in cancer cells and podocytes under nutrient-deprived conditions.[20,21] Similarly, phosphorylated FoxO1 leads to its cytoplasmic retention, initiating autophagy through interaction with ATG7.[22,23] Moreover, FoxO1 has also been implicated in regulating autophagy in skeletal muscle to maintain muscle mass and function, particularly during nutrient deprivation.[24–26] However, the mechanisms governing subcellular localization of FoxO1 in myogenic progenitors are not well understood.

Protein arginine methyltransferases (PRMT1–9) are enzymes that mediate the transfer of a methyl group to an arginine (R) residue in substrate proteins. PRMTs regulate a wide range of biological processes, including gene expression, protein localization, and signal transduction, in skeletal muscles through regulating the methylation status of key proteins responsible for the homeostasis of SCs.[27,28] Emerging studies have demonstrated that arginine methylation, mediated by PRMTs, also regulates SC function *in vivo*.[27] For example, PRMT1 methylates SIX1 to control *MyoD* expression, thereby promoting SC proliferation and enhancing muscle regeneration.[29] Similarly, PRMT4, also known as CARM1, has been reported to modulate the asymmetric division of SCs and autophagy through Pax7 methylation.[30] PRMT7 is recognized not only as an epigenetic regulator that maintains the regenerative capacity of SCs through DNMT3b/p21 axis but also as a promoter of SC differentiation through p38MAPK methylation.[31,32] A recent study reported

that PRMT5 plays a critical role in SC proliferation and adult muscle regeneration by regulating postnatal day (P) 21 via an unknown mechanism.[33] However, it remains unknown whether and how PRMT5 plays a role in embryonic myoblasts and muscle development.

To gain insight into the physiological function of PRMT5 in myogenesis, we generated a conditional knockout (KO) mouse using *MyoD*^{Cre} to drive the deletion of the *Prmt5* allele in embryonic myoblasts (referred to as *Prmt5*^{MKO}). Our investigation revealed that the *Prmt5*^{MKO} mice exhibited a significant reduction in skeletal muscle mass and contractile function, accompanied by immune cell infiltration. Further analysis uncovered a link between muscle atrophy and early developmental defects, attributed to diminished myoblast proliferation and premature differentiation. Notably, the *Prmt5*-null myoblasts had elevated cytoplasmic FoxO1 levels, associated with autophagy activation and subsequent depletion of lipid droplets within the myoblasts. Accordingly, pharmacological inhibition of autophagy normalized lipid content and partially restored muscle regeneration in the *Prmt5*^{MKO} mice. Collectively, our study establishes the role of PRMT5 as a regulator of autophagy in SCs, which subsequently affects muscle development and repair.

RESULTS

Adult *Prmt5*^{MKO} mice exhibit muscle atrophy and early lethality

To investigate the roles of PRMT5 in myogenic progenitors *in vivo*, we generated a myogenic lineage-specific conditional *Prmt5* KO mice (abbreviated as *Prmt5*^{MKO}) by crossing *Prmt5*$^{flox/flox}$ mice with *MyoD*^{Cre} mice expressing Cre recombinase under the control of the *Myod1* gene promoter. In this mouse model, the deletion of exon 7 in the Prmt5 gene causes a frameshift and premature stop codon, resulting in a truncated protein without any essential functional domains.[34] Real-time qPCR validated the efficient depletion of *Prmt5* in skeletal muscles in *Prmt5*^{MKO} mice (Figure S1A).

Morphologically, the *Prmt5*^{MKO} mice appeared smaller than wild-type (WT) littermates, as indicated by significantly lower body weights than WT siblings at all examined time points (Figures 1A and S1B). The body weight differences between WT and *Prmt5*^{MKO} mice became more prominent with age (Figure 1B). As a consequence, the *Prmt5*^{MKO} mice failed to thrive after 4 months, with all dying before 18 weeks of age (Figure 1C). EchoMRI analysis confirmed that the *Prmt5*^{MKO} mice exhibited a significantly lower average lean mass than their WT littermates, without significant alternation in fat mass (Figure 1D). The size and weight of various muscle groups, including *soleus* (SOL), *extensor digitorum longus* (EDL), *tibialis anterior* (TA), *gastrocnemius* (GAS), *quadriceps* (QU), and diaphragm (Di) were noticeably reduced in the *Prmt5*^{MKO} mice compared to their WT littermates (Figures 1E and S1C). We further analyzed TA muscle cross sections with myofiber boundaries (sarcolemma) marked by an antibody against dystrophin. The myofiber cross-sectional area (CSA) distribution showed an increased proportion of small myofibers and diminished large myofibers in the *Prmt5*^{MKO} TA, resulting in a significantly smaller average myofiber size (Figures 1F–1H). Total numbers of myofiber per TA muscle were also reduced in the *Prmt5*^{MKO} mice (Figure 1I). To assess the impact of *Prmt5* deletion on motor function, we conducted treadmill and grip strength tests. The *Prmt5*^{MKO} mice showed significantly diminished running time, maximum speed, and running distance, as

well as reduced grip strength, compared to their WT littermates (Figures 1J–1M). We also directly evaluated muscle force of EDL and SOL muscles from WT and *Prmt5*^{MKO} mice and observed that *Prmt5*^{MKO} muscles exhibited lower absolute force (Figures 1L and 1M) and specific force (Figures 1N and 1O).

We also performed pathological analysis of skeletal muscles from both *Prmt5*^{MKO} and littermate control mice. H&E staining revealed that the *Prmt5*^{MKO} TA muscles contained numerous centrally nucleated myofibers (CNFs) (Figure S1D, asterisks), a defining characteristic of myopathy. In addition, the *Prmt5*^{MKO} Di muscles exhibited an accumulation of interstitial mononuclear cells and were visibly thinner compared to WT muscles (Figure S1E). Furthermore, an elevated number of IgM^{+} myofibers and CD68^{+} cells, markers for degenerating myofibers and infiltrated macrophages/monocytes, respectively, were detected in the *Prmt5*^{MKO} muscles, indicative of inflammation (Figures S1F and S1G). To further substantiate our findings, we quantified several immune cell markers in mononuclear cells dissociated from hindlimb muscles using fluorescence-activated cell sorting (FACS). The *Prmt5*^{MKO} muscles contained a significantly higher population of immune cells (CD45^{+}, CD11b^{+}, MHCII^{+}, F4/80^{+}) compared to WT muscles (Figures S1H and S1I). Collectively, these results demonstrate that myogenic line-age-specific ablation of *Prmt5* leads to age-dependent decline in muscle size and contractile function, accompanied by pathogenic myopathy and chronic inflammation.

Prmt5^{MKO} diminishes SCs and their regenerative capacity in adult mice

As SCs are derived from embryonic myoblasts, we further explored whether the deletion of *Prmt5*^{MKO} affects the generation of SCs.[35] Using FACS, we isolated SCs from the hindlimb muscles of WT and *Prmt5*^{MKO} mice, revealing a significantly lower abundance of SCs in the *Prmt5*^{MKO} mice (Figure S2A). RT-qPCR analysis demonstrated reduced *Pax7* and elevated *Myog* mRNA levels in the *Prmt5*^{MKO} muscles (Figure S2B). Consistently, immunofluorescence staining confirmed that the *Prmt5*^{MKO} muscles had significantly lower numbers of Pax7^{+} SCs and an increased numbers of MyoG^{+} differentiating cells (Figures S2C and S2D). Similarly, staining for Pax7 in freshly isolated myofibers revealed fewer Pax7^{+} cells and myonuclei per myofiber in the *Prmt5*^{MKO} myofibers (Figures S2E–S2G). In contrast, a higher proportion of myofiber-associated SCs expressed MyoG in *Prmt5*^{MKO} mice (Figure S2H), and the *Prmt5*-deficient myoblasts fused poorly despite normal differentiation (Figure S2I). These results demonstrate an essential role of PRMT5 in maintaining SCs, as the *Prmt5*^{MKO} SCs undergo spontaneous differentiation in adult muscles.

To assess the functionality of the remaining *Prmt5*-null SCs, we examined the regeneration of TA muscles following cardiotoxin (CTX)-induced injury (Figures S3A and S3B). Histological analyses revealed that the *Prmt5*^{MKO} muscles displayed severe inflammatory infiltration, resulting in 21% and 39% reductions in the recovery rate compared to WT muscles at 5 and 21 days post injury (DPI), respectively (Figure S3C). Immunohistochemistry also demonstrated a significant reduction in the number of Pax7^{+} cells, and MyoG^{+} cells, as well as in the newly regenerated myofibers surrounded by laminin in the *Prmt5*^{MKO} mice at 5 DPI (Figures S3D and S3E). At 21 DPI, a reduced

number of Pax7$^+$ cells and an increase in MyoG$^+$ cells were detected in the *Prmt5*^{MKO} muscles, but regenerated laminin-surrounded myofibers were observed in both WT and KO muscles (Figures S3F and S3G). The initial lack of regenerated myofibers at 5 DPI followed by eventual catch-up at 21 DPI suggest a delay in the regeneration process. Taken together, these results indicate that PRMT5 in embryonic myoblasts plays a critical role in the generation of SCs, and continued expression of PRMT5 is necessary for the efficient regenerative capacity of the SCs.

Prmt5^{MKO} impairs SC proliferation and delays muscle growth and maturation

Given the reduced number of SCs and myonuclei in *Prmt5*^{MKO} mice (Figures S2F and S2G), we hypothesized that PRMT5 in SCs may be crucial for myonuclei accretion during postnatal growth. To test this hypothesis, we examined WT and *Prmt5*^{MKO} mice during early postnatal muscle growth (P7, P14). We observed fewer Pax7$^+$ cells and more MyoG$^+$ cells at P7 and P14 in *Prmt5*^{MKO} muscles (Figures 2A and 2B), suggesting reduced proliferation and premature differentiation of these *Prmt5*-null myogenic progenitors. Interestingly, we also noticed numerous nascent eMyHC$^+$ myofibers in the *Prmt5*^{MKO} muscles, which were rarely detectable in WT muscles at P7 (Figure 2C), indicating a delayed postnatal maturation or formation of myofibers. Immunoblotting analysis not only confirmed the robust upregulation of eMyHC proteins in the *Prmt5*^{MKO} muscles at P7 but also revealed diminished protein contents of MyoD in the *Prmt5*^{MKO} muscles at both P7 and P14 (Figures 2D and 2E). As MyoD marks proliferating myoblasts (non-quiescent SCs) in growing muscles, the diminished MyoD level demonstrates proliferation defects of the *Prmt5*^{MKO} SCs. These findings collectively suggest that PRMT5 is indispensable for SC proliferation and early postnatal muscle growth and maturation, resulting in a significant reduction in body weight in the *Prmt5*^{MKO} relative to WT mice (Figure 2F).

PRMT5 is essential for embryonic and perianal myogenesis

A reduced number of Pax7$^+$ SCs at P7 suggests a defect in the generation of myoblasts and SCs during embryonic myogenesis in the *Prmt5*^{MKO} mice. To explore the involvement of PRMT5 in the early stages of myogenesis, we analyzed hindlimb muscles of WT and *Prmt5*^{MKO} mice during embryonic and perinatal myogenesis. We observed a significant decrease in body size and body weight of *Prmt5*^{MKO} newborn mice (P1) compared to WT littermates (Figure 3A). Immunofluorescence analysis revealed reduced proliferating SCs (calculated by proportions of Pax7$^+$Ki67$^+$ cells among all Pax7$^+$ cells) and increased MyoG$^+$ cells in KO muscles (Figures 3B and 3C). Additionally, hindlimb muscles of E18.5 *Prmt5*^{MKO} mice were smaller with fewer Pax7$^+$ cells and more MyoG$^+$ cells compared to their WT littermates (Figures 3D–3G).

To further investigate the effects of PRMT5 on SC proliferation, we established myoblasts from tamoxifen (TAM)-inducible *Prmt5*$^{flox/flox}$/*Rosa*^{CreER} mice and treated the cells with 4-hydroxy-tamoxifen (4-OH) to induce *Prmt5* deletion, or with methanol (MeOH) as vehicle control. We found a significant reduction in Ki67$^+$ cells in 4-OH treated (*Prmt5*-KO) myoblasts compared to MeOH-treated control cells (Figure 3H). Furthermore, EdU (5-ethynyl-2′-deoxyuridine) labeling of proliferating cells on cultured single myofibers revealed significantly lower percentages of EdU$^+$Pax7$^+$ SCs on *Prmt5*^{MKO} myofibers

relative to WT myofibers (Figures 3I and 3J). Taken together, these results demonstrate that PRMT5 plays an important role in maintaining embryonic and perinatal myogenesis, and its deletion hinders proliferative capacity of myoblasts and impairs muscle development.

Prmt5^{MKO} alters lipid metabolism and impairs SC fate homeostasis

PRMT5 has been shown to regulate lipid metabolism in adipocytes and skeletal muscles.[34,36] We have recently identified LD as an important metabolic regulator of SC fate,[14] we therefore explored whether PRMT5 regulates SCs through LDs. We utilized oil red O (ORO) staining to visualize and quantify LD contents in myoblasts. The *Prmt5*-null myoblasts exhibited a remarkably reduced intensity of ORO^{+} LDs (Figure 4A). Immunofluorescent staining of LDs by BODIPY also revealed a decreased intensity of LDs in *Prmt5*-KO compared to WT myoblasts (Figure 4B). Additionally, using the myofiber explant model, we observed that SCs on 72-h-cultured single myofibers isolated from *Prmt5*^{MKO} mice failed to accumulate LDs, while WT SCs accumulated many LDs (Figure 4C). Diminished LD content was associated with upregulation of lipolysis gene (*Pnpla2*) and downregulated genes related to lipid synthesis (*Fabp4, Dgat1*) in *Prmt5*-null myoblasts (Figure 4D).

To investigate whether LD reduction in the Prmt5-null cells alters SC fate, the SCs were stained with Pax7 and MyoD antibodies (Figure 4E). In *Prmt5*-null myofibers, there was not only a reduction in the number of cells per cluster but also a significant decrease in Pax7^{+}/MyoD^{-} (self-renewing) cells, accompanied by an increase in the proportion of Pax7^{-}/MyoD^{+} (differentiating) cells (Figures 4F and 4G). To evaluate the energetic consequence of LD reduction in *Prmt5*-null myoblasts, we used Seahorse bioanalyzer to determine the oxygen consumption rate (OCR) (Figure 4H). The results showed a significant decrease in OCR for basal respiration, proton leak, ATP respiration, maximal respiration, and non-mitochondrial respiration in *Prmt5*-null myoblasts compared to WT cells (Figures 4H and 4I). These findings indicate that *Prmt5*^{MKO} alters lipid metabolism and oxygen-dependent cellular bioenergetics in SCs, disrupting the homeostasis of SC fate.

Prmt5^{MKO} myoblasts exhibit elevated autophagy

We next explored the molecular mechanism responsible for the depletion of LDs and spontaneous differentiation of *Prmt5*^{MKO} SCs. Previous work indicated that autophagy plays a critical role in both lipid catabolism and SC activation from quiescence.[12,37] To investigate the potential role of PRMT5 in regulating myoblast autophagy, we exposed both WT (MeOH treated) and KO (4-OH treated) *Rosa26*^{CreER}/*Prmt5*$^{flox/flox}$ myoblasts to a 3-h serum withdrawal to induce autophagy in the presence or absence of the autophagy inhibitor, hydroxychloroquine (HCQ). Compared to WT myoblasts, the *Prmt5*-KO myoblasts exhibited a notable increase in LC3-lipidation, indicated by the LC3 II/LC3 I ratios (Figure 5A). Notably, the elevated LC3 II/I ratio in *Prmt5*-KO myoblasts was normalized by HCQ (Figure 5A), indicating that *Prmt5* KO promotes autophagy. To exclude the possibility that autophagy and LD depletion are induced by the 4-OH treatment, we treated myoblasts derived from *Rosa26*^{CreER}/*Prmt5*$^{flox/+}$ mice with MeOH or 4-OH. No significant differences were observed in the autophagic response (LC3BII/I levels) or LD content (Bodipy intensity) in myoblasts, excluding a role of 4-OH (Figures S4A and S4B).

The *Prmt5*^{MKO} myoblasts also showed higher mRNA levels of autophagy-related genes (LC3B, Lamp1, Ulk1, Beclin1, Atg7) compared to WT myoblasts (Figure 5B). Moreover, the average intensity of LC3B immunofluorescence in *Prmt5*-null SCs was higher than that of WT SCs attached to freshly isolated single myofibers (Figure 5C). These results illustrate that *Prmt5*^{MKO} activates autophagy in SCs.

PRMT5 mediates FoxO1 methylation to modulate its subcellular localization

We next sought to understand how PRMT5 regulates autophagy. Forkhead box protein O1 (FoxO1) is a transcriptional factor that, when sequestrated in the cytoplasm, induces autophagy.[38] Interestingly, we observed that *Prmt5*^{MKO} resulted in increased levels of cytoplasmic FoxO1 (Figure 6A). Additionally, we performed immunofluorescence staining of FoxO1 in SCs on freshly isolated myofibers (Figure 6B). While FoxO1 expression was predominantly localized to the nucleus in WT SCs (nearly 100%), approximately 65% of *Prmt5*^{MKO} SCs exhibited nuclear FoxO1, with 35% of SCs showing cytoplasmic FoxO1 distribution (Figure 6B). These results provide an unexplored function of PRMT5 in regulating the subcellular distribution of FoxO1 in SCs.

We then performed a series of biochemical analyses to further understand how PRMT5 regulates subcellular localization of FoxO1 in SCs. We investigated the potential protein interaction between FoxO1 and PRMT5 and whether or not PRMT5 mediates FoxO1 methylation to alter its subcellular localization. A co-immunoprecipitation (coIP) experiment revealed that, compared to the control (MeOH) group, *Prmt5* deletion (4-OH) significantly reduced the dimethylation of FoxO1, marked by the SYM10 antibody (Figures 6C and 6D). However, a direct interaction between PRMT5 and FoxO1 was not detected (Figures 6C and 6E). To explore the effect of *Prmt5* KO on the intracellular localization of FoxO1, we conducted coIP following cellular fractionation. Remarkably, *Prmt5* KO only reduced the levels of methylated FoxO1 in the nucleus, without significantly altering FoxO1 methylation in the cytoplasm, resulting in a higher level of total cytoplasmic FoxO1 (Figures 6F–6H). Conversely, the overexpression of *Prmt5* led to enhanced FoxO1 methylation, and pharmacological inhibition of PRMT5 using BLL3.3 decreased FoxO1 methylation in C2C12 myoblasts (Figures S5A and S5B). To further verify the involvement of PRMT5 in FoxO1 methylation and its potential interaction with FoxO1, we employed *in situ* proximity ligation assay (PLA), a technique that enables the visualization of colocalized proteins within 40 nm as puncta signal. The results confirmed colocalization of symmetric demethylated protein and FoxO1 in the nucleus of WT myoblasts but not in KO myoblasts (Figure 6I). However, we did not observe PLA signals of PRMT5 and FoxO1 in either WT or KO myoblasts (Figure 6J) To investigate the biological significance of PRMT5-mediated FoxO1 methylation, we conducted FoxO1 protein stability assay after the addition of cycloheximide (CHX) in control (MeOH) and KO (4-OH) C2C12 myoblasts. The results revealed that FoxO1 stability was increased over time in the KO group (Figure S5C), indicating that PRMT5-mediated methylation destabilizes FoxO. Overall, these findings suggest that PRMT5 governs the methylation of nuclear FoxO1 and *Prmt5*-KO leads to the accumulation of FoxO1 in the cytoplasm.

To directly examine the role of cytoplasmic FoxO1 in autophagy, we transfected C2C12 myoblasts with different constructs, including an empty vector (EV), WT FoxO1, a cytoplasmic FoxO1 mutant lacking the DNA binding domain (ΔDB), and a variant of ΔDB with mutations in the three AKT phosphorylation sites (ΔDB3A) that promote nuclear localization (Figure S6A). Immunoprecipitation-western blot analysis revealed that myoblasts transfected with WT or ΔDB had elevated autophagy, as indicated by LC3II/LC1 ratio, and increased association between FoxO1 and autophagy initiation factor ATG7, as compared to ΔDB3A-transfected myoblasts (Figures S6B and S6C). Subsequently, we only detected the interaction between FoxO1 and ATG7 in the cytoplasm of primary myoblasts, but not in the nucleus (Figure S6D). Collectively, these findings provide substantial evidence that cytoplasmic FoxO1 associates with ATG 7 to modulate autophagic activity in muscle cells.

Pharmacological inhibition of autophagy partially rescues *Prmt5*^{MKO} myoblasts

As inhibition of autophagy increases lipid content,[37,39] we tested whether inhibition of autophagic flux with HCQ could rescue the lipid content and function of *Prmt5*-null myoblasts (Figure 7A). This treatment led to an increased intensity of LDs in both WT and *Prmt5*-null myoblasts, with a more significantly robust increase in KO cells (Figure 7B). Furthermore, HCQ treatment remarkably upregulated the expression of the lipid metabolism marker (*Dgat1*), while simultaneously suppressing the autophagic marker LC3B in *Prmt5*-null SCs (Figure 7C).

We also examined the effect of autophagy inhibition on SCs attached on myofibers isolated from WT and *Prmt5*^{MKO} mice. Immunostaining with Bodipy no significant changes in LD abundance in SCs of HCQ-treated WT myofibers, while *Prmt5*-deficient SCs exhibited increased LD abundance in response to HCQ (Figure 7D). These results suggest that the inhibition of autophagy flux by HCQ rescues lipid contents in Prmt5-null SCs. To assess whether HCQ rescues Prmt5-null SCs *in vivo*, we treated WT and *Prmt5*^{MKO} mice with HCQ via daily intraperitoneal injections for 14 days. We then performed CTX-induced muscle injury, followed by 7 days of recovery, during which HCQ was continuously injected (Figure 7E). While HCQ treatment did not result in significant differences in muscle morphology of WT mice, noticeable improvement in muscle regeneration were observed in *Prmt5*^{MKO} mice. Specifically, HCQ treatment led to a 30% increase in the average size of laminin^{+} myofibers in the *Prmt5*^{MKO} mice (Figures 7F–7H). However, the overall recovery of the HCQ-treated *Prmt5*^{MKO} muscles was still worse than the WT muscles (Figures 7F–7H), indicating that HCQ only partially restores muscle regeneration in the *Prmt5*^{MKO} mice.

DISCUSSION

Our study delineates a physiological role of PRMT5 in myoblasts during muscle development, growth, and regeneration. We provide compelling evidence that PRMT5 mediates FoxO1 methylation and controls subcellular localization to regulate lipophagy in myoblasts. Our findings suggest that PRMT5-mediated methylation of FoxO1 in the nucleus promotes nuclear retention and transcriptional activity of FoxO1, influencing the expression of genes involved in lipogenesis. In the absence of PRMT5, FoxO1 is sequestered in the

cytoplasm, which triggers autophagy along with the spontaneous differentiation of SC and results in impaired muscle regeneration. Subsequently, the pharmacological inhibition of autophagy using HCQ treatment effectively restores lipid content and partially enhances muscle regeneration in *Prmt5*^{MKO} SCs.

Our study employed *MyoD*^{Cre} mice, genetically engineered to specifically target embryonic myoblasts, to investigate the impact of *Prmt5* deletion on muscle development. A previous study has shown that loss of *Prmt5* using *Pax7*^{Cre} mice did not affect embryonic myogenesis but leads to premature death, presumably due to off-target deletion of *Prmt5* in the central nervous system.[33,40,41] Consistently, PRMT5-mediated histone modifications are crucial for neurogenesis in neural stem cells (NSCs) and conditional deletion of *Prmt5* in NSCs and oligodendrocytes leads to premature death.[42–44] The lack of effect on myogenesis in the *Pax7*^{Cre}-driven *Prmt5* KO mice may be explained by the compensatory role of *Pax3*-lineage myogenic cells in myogenesis. The *Pax* genes, including *Pax3* and its paralog *Pax7*, are known to play crucial roles in the myogenesis process by activating the transcription of myogenic regulatory factors.[45,46] Previous mouse studies have shown that *Pax3* expression (E8) is initiated earlier than *Pax7* expression (E9) during embryonic myogenesis, and the majority of myogenic cells in the limb are derived from Pax3^{+} cells.[47,48] While *Pax7* has been recognized as essential for adult myogenesis and regeneration, its role in fetal myogenesis is limited or may be compensated by other proteins.[49–51] Utilizing *MyoD*^{Cre}-mediated deletion of *Prmt5* provides distinct advantages to investigate myogenesis of muscle progenitors, as *MyoD* is intimately involved in the developmental pathway during fetal myogenesis.[45,46] Moreover, PRMT5 is required for the interaction between Brg1 and MyoD, which plays a crucial role in regulating muscle differentiation.[52] Our finding suggests that leveraging the *MyoD*^{Cre}-mediated ablation of PRMT5 is a valuable *in vivo* tool for elucidating the role of PRMT5 in myogenesis. This approach led to the discovery of a key role of PRMT5 in embryonic myogenesis.

Emerging studies have highlighted the critical role of LDs in the behavior and fate of SCs, and the availability of LDs through *de novo* lipogenesis is implicated in NSC proliferation.[14,53,54] PRMTs have been reported to modulate lipid metabolism and influence cellular activity in various tissues. For instance, PRMT1 has been shown to facilitate proliferation through its interaction with C/EBPβ during adipocyte differentiation, and PRMT3-mediated methylation of LDHA (lactate dehydrogenase A) promotes glycolysis, a key process in lipid metabolism, thereby influencing tumor growth.[55,56] Moreover, PRMT5 has been implicated in facilitating fatty acid biogenesis by methylating mSREP1a and enhancing LD formation through SPT methylation, which subsequently interacts with Bscl2 in adipocytes.[34] Despite the established role of PRMT5 in SC proliferation,[33] the molecular mechanisms underlying the defective proliferation of *Prmt5*-KO SCs are not well understood. In our study, we observed that PRMT5 deletion led to a reduction in LD content, which resulted in impaired SC proliferation, but promoted spontaneous SC differentiation, accompanied by compromised energy production. Rhabdomyosarcoma, a solid tumor originating in muscle tissues, is associated with high frequencies of Pax7^{+} SCs.[57,58] Our study suggests that targeting PRMT5 may diminish the population of proliferating SCs, thereby inhibiting the growth of rhabdomyosarcoma.

Autophagy is a key player in regulating the homeostasis of skeletal muscles, and it triggers the proliferation of SCs by boosting energy supply.[59] *In vivo* studies involving the pharmacological and genetic inactivation of *Sirt1* have revealed that autophagy is induced during SC activation.[12] Moreover, several studies have highlighted the role of autophagy in modulating intracellular lipid reserves through a process known as lipophagy.[8,15,37] A recent study has indicated that autophagy is critical for removing intramyocellular triglycerides in myocytes.[15] Our study supports the finding that the loss of PRMT5 triggers autophagy, accompanied by LD clearance. Moreover, we observed an elevation in LD contents in *Prmt5*-null SCs upon treatment with an autophagy inhibitor, which could potentially explain the augmented muscle repair capacity observed in $Prmt5^{MKO}$ mice. Dysfunctions in autophagy have been observed in various myopathies.[26,59] The use of a small molecule to promote autophagy activation has shown promise in enhancing muscle regeneration and ameliorating a spectrum of myopathy and DMD (Duchenne muscular dystrophy) conditions.[13,60,61] On the other hand, the impaired muscle regeneration observed in *Islr*-null muscle was effectively rescued by genetic deletion of *Dcat1/Islr*, which antagonized autophagy activation.[62] Furthermore, an *in vivo* study has demonstrated that the inhibition of the autophagy pathway remarkably ameliorates pathology associated with congenital muscular dystrophy caused by laminin α2 chain deficiency (MDC1A).[63] Muscle regeneration is an intricate process involving coordinated action of multiple cell types.[35] Circulating cytokines/chemokines secreted from immune cells can facilitate the activation of SCs to replace damaged tissue, and autophagy serves as a crucial regulator to either enhance or suppress the immune response.[64,65] Hence, it is essential to have a dedicated mechanism to control autophagy in SCs at an appropriate level. Our results identify PRMT5 as a negative regulator (or inhibitor) of autophagy in myoblasts.

The protein FoxO1 plays a critical role in regulating autophagy by promoting the expression of several key genes to maintain cellular homeostasis.[66,67] Emerging studies have shown that FoxO1 activity and localization within cells are tightly controlled by PTMs.[22,68] Phosphorylation of specific residues on FoxO1 by kinases such as AKT and serum/glucocorticoid regulated kinase 1 (SGK1) leads to its retention in the cytoplasm, inhibiting its transcriptional activity.[69,70] Conversely, dephosphorylation of FoxO1 by PP2a promotes its nuclear translocation, inducing the expression of its target genes.[71,72] Furthermore, under stress conditions, acetylated FoxO1 associates with ATG7 in the cytoplasm, initiating the autophagic process.[20] These findings highlight the significance of PTMs in regulating function and localization of FoxO1. Besides phosphorylation and acetylation, FoxO1 also undergoes lysine methylation mediated by G9a, which controls its protein stability.[73] Furthermore, PRMT1 was reported to methylate FoxO1 on arginine residues 248 and 250, which subsequently inhibits the phosphorylation of FoxO1 at serine 253.[38] Our study revealed that PRMT5-mediated methylation subsequently prevents the translocation of FoxO1 to the cytoplasm. In the absence of PRMT5, FoxO1 remains sequestered in the cytoplasm, leading to changes in the cellular function of SCs. This is supported by another study reporting that SC-specific *Pten*-KO resulted in nuclear exclusion of FoxO1, indicating that cytoplasmic FoxO1 promotes exhaustion of quiescent SCs.[16]

Our study sheds light on the significant function of PRMT5 in regulating autophagy as a means of lipid catabolism (lipophagy), an area of growing interest due to its

potential implications in metabolic syndrome.[74,75] Specifically, our findings elucidated the importance of PRMT5-mediated methylation of FoxO1 in the nucleus, which is essential for maintaining muscle development. Nevertheless, the precise molecular mechanism underlying the downstream targets of FoxO1 in SCs remains uncertain. A previous study has reported that FoxO1 binds to the promoter of PGC1α, modulating fatty acid catabolism in the liver under stress conditions.[25] Moreover, the activation of FoxO1 can bind to the promoter region of the *Pnpla2* gene (encoded by ATGL protein), resulting in elevated triglyceride breakdown for energy production.[76] These findings suggest that there may be multiple potential regulatory factors involved in the PRMT5-FoxO1 axis signaling pathway, which could affect lipophagy in SCs. Understanding these mechanisms is essential for exploring the role of PRMT5 in the context of SC function for muscle development and regeneration.

Limitations of the study

While our myogenic-specific conditional KO mice reveal a physiological role of PRMT5 in myogenesis, the underlying mechanisms remain to be fully elucidated. We provided evidence that *Prmt5* KO induces cytoplasmic accumulation of FoxO1, which is associated with the autophagy initiation factor ATG7, elevates autophagic activities, and reduces LD content. However, pharmacological inhibition of autophagy using HCQ only partially restored muscle regeneration in the $Prmt5^{MKO}$ mice following muscle injury. This may represent a key limitation of the systemic delivery of HCQ, which could influence many other cell types beyond SCs. For example, HCQ has been shown to modulate the function of both innate and adaptive immune cells,[77,78] which have been reported to play key roles in muscle regeneration.[79] In this context, it is not surprising that HCQ treatment has been shown to promote muscle atrophy in humans.[80,81] In our study, while the systemic HCQ treatment restored LD contents and perhaps the regenerative function of SCs, its off-target effect on other cell types may have largely negated the positive effects on SCs, resulting in only partial rescue of overall regeneration. Indeed, our recent study has demonstrated that myofiber-specific restoration of LDs rescues the phenotype of myofiber-specific *Prmt5*-KO mice very effectively.[82] Future studies should explore the possibility of targeted delivery of HCQ into muscle cells using for example nanoparticle delivery tools.[83,84]

STAR★METHODS

RESOURCE AVAILABILITY

Lead contact—Further information an inquiries regarding resources and reagents should be directed to the Lead Contact, Shihuan Kuang, Ph.D (skuang@purdue.edu)

Materials availability—All unique/stable reagents generated in this study are available from the lead contact with a completed materials transfer agreement.

Data and code availability

- Data reported in this paper will be shared by the lead contact upon request.
- This paper does not report original code.

- Any additional information required to reanalyze the data reported in this paper is available from the lead contract upon request.

EXPERIMENTAL MODEL AND STUDY PARTICIPANT DETAILS

Animals—All mouse procedures were approved by the Purdue University Animal Care and Use committee. *Prmt5*$^{flox/flox}$ mice were generously provided by Chengdeng Hu (Purdue University), and other mice strains were acquired from Jackson Laboratory using the following stock numbers: *MyoD*^{Cre} (stock# 014140) and *Rosa26*^{CreER} (stock# 008463). The mice were housed in the animal facility with free access to standard rodent chow food and water. Unless otherwise noted, 8- to10-week-old mice of both sexes (male and female) were used in this study.

Primary myoblast isolation and culture—Primary myoblast derived from hindlimb muscles of 4-week-old WT and *Rosa*^{CreER}/*Prmt5*$^{f/f}$ mice (male and female) were minced and then digested using a type II collagenase and Dispase B mixture (Roche).[85] Digestion was neutralized by adding growth media containing F-10 Ham's medium (Thermo Fisher Scientific), 20% fetal bovine serum (FBS), 1% penicillin, 4 ng/mL basic fibroblast growth factor (Thermo Fisher Scientific), and the cells were cultured on collagen-coated plates. Primary myoblasts were then purified using pre-plating, which was performed 2–3 times. For *in vitro* genetic deletion, the myoblasts were treated with 4-hydroxyl Tamoxifen (4-OH, 0.4 μM) for 4 days to induce Cre-mediated deletion, while methanol (MeOH) was used as a vehicle control.

Single myofiber isolation and culture—Single myofibers were extracted from EDL muscles of WT and *Prmt5*^{MKO} mice. briefly, EDL muscles were meticulously dissected and placed in a digestion medium containing 1.5 mg/mL collagenase I in Dulbecco's Modified Eagle's Medium (Sigma, DMEM) and incubated for a specific time (WT for 50 min and *Prmt5*^{MKO} for 80 min) at 37°C subsequently, the EDL muscles were carefully transferred to a pre-heated plate containing 5 mL of DMEM, and single myofibers were released by flushing the muscles gently with a large pore glass pipette. The released single myofibers were then transferred, cultured in culture plate (60 mm) coated with horse serum and incubated in DMEM supplemented with 20% FBS (HyClone), 4 ng/mL basic FGF (Promega), and 1% penicillin-streptomycin (Hyclone) at 37°C. The myofibers were collected at specific time points for further analysis.

METHOD DETAILS

Muscle injury and drug treatment—Muscle injury was induced by injecting 50 μL of CTX (Sigma, 10 μM) dissolved in saline into TA muscle. Muscles were harvested at the indicated days post injection to evaluate the completion of regeneration. For preparation of Hydroxychloroquine (HCQ, TCI, H1306), it was dissolved in saline at 10 mg/mL. Prior to CTX injury, a dose of 50 mg/kg (50 mpk) was administrated by intraperitoneal (IP) injection daily for a period of two weeks. Recovery rate is determined by calculating the ratio of the injured muscle weight to the uninjured muscle weight.

Histology and immunofluorescence staining—Whole muscle tissues or TA muscle from WT and *Prmt5*^{MKO} mice were frozen in an optimum cutting temperature (OCT) compound. A Leica CM 1850 cryostat was employed to cross-section the frozen muscles into 10 μm sections. These sections were then subjected to H&E staining or immunofluorescence staining. For immunofluorescent staining, briefly, samples including cross-sections, single myofibers, and primary myoblasts were fixed in 4% paraformaldehyde (PFA) for 15 min, followed by quenching with 100 mM glycine for 10 min. Samples were then incubated in blocking buffer, which contained 5% goat serum, 2% BSA, 0.2% Triton C-100 and 0.1% sodium azide, for 2 h. The samples were then incubated with primary antibodies at the indicated ratio, followed by incubation with secondary antibody.

Body composition analysis measurement—The body composition of live mice was measured using the Echo-MRI 130 analyzer (EchoMRI LLC, Houston, Tx, USA). The instrument was calibrated with corn oil prior to use. The mouse was then gently placed into a cylindrical holder, which was inserted into the EchoMRI system to measure lean mass.

Measurement of treadmill, grip strength test and muscle contractile function—Prior to the treadmill exercise test, WT and *Prmt5*^{MKO} mice were trained on a treadmill (Eco3/6; Columbus Instruments, Columbus, OH) set at a constant speed of 10 m/min for 5 min per day for 3 consecutive days. On the day of the exercise test, the mice were subjected to the treadmill at 10 m/min for 5 min, after which the speed was increased by 2 m/min every 2 min until the mice reached exhaustion. Excise capacity including running time, running distance, and maximum speed were then analyzed.

To measure the gripping strength, a digital grip strength meter was employed (Columbus Instruments). The mouse grasped the grid, and its tail was gently pulled along the axis the grid to record peak tension at the time of release. The grip strength was assessed in three trials, each repeated fifteen times, and the average strength was normalized to body weight (N/g).

For the assessment of the contractile properties of slow-twitch Soleus and fast-twitch EDL muscles, we employed an *ex vivo* muscle test system (Aurora Scientific, 1200A intact Muscle Test System). The hindlimb of mice (anesthetized with isoflurane) was excised and placed in a bicarbonate-buffered solution. Braided silk suture thread (Fine Science Tools, 4–0) was tied around each end of the muscle tendons, the muscles were mounted between two platinum electrodes in a tissue bath apparatus containing a bicarbonate-buffered solution at room temperature. To generate the force-frequency relationship, we select frequencies between 1 and 300 Hz for the EDL muscle and 1–200 Hz for the Soleus muscle. Once the contractile properties of the muscles were measured, the muscles were removed from the organ bath, freed from the connective tissue, dried with a blotting paper, and weighed. We determined the muscle cross-sectional area (CSA) by dividing the wet muscle mass by the product of Lo and muscle-specific density (1.056 g/cm^3). To calculate the specific force (N/cm^2), we divided the muscle force (N) by the CSA (cm^2).

Primary myoblast isolation, culture, and flow cytometry analysis—Primary myoblasts derived from hindlimb muscles of 4-week-old WT and *Rosa*^{CreER}/*Prmt5*$^{f/f}$

mice were minced and then digested using a type II collagenase and Dispase B mixture (Roche).[85] Digestion was neutralized by adding growth media containing F-10 Ham's medium (Thermo Fisher Scientific), 20% fetal bovine serum (FBS), 1% penicillin, 4 ng/mL basic fibroblast growth factor (Thermo Fisher Scientific), and the cells were cultured on collagen-coated plates. Primary myoblasts were then purified using pre-plating, which was performed 2–3 times. For *in vitro* genetic deletion, the myoblasts were treated with 4-hydroxyl Tamoxifen (4-OH, Sigma, 0.4 μM) for 4 days to induce Cre-mediated deletion, while methanol (MeOH) was used as a vehicle control.

For flow cytometry, primary myoblast isolation was conducted.[86] In brief, hindlimb muscles from both WT and *Prmt5*^{MKO} mice were minced and digested with type II collagenase (700 U/ml) at 37 for 60 min. The samples were then centrifuged, and additional digestion solution (100 U/ml type II collagenase and 1 U/ml Dispase II) was added, followed byincubation at 37°C for 30 min. The resulting samples were filtered through 40-μm cell strainers and washed with F-10 HAM's medium containing 10% horse serum and 1% penicillin-streptomycin (Hyclone). The suspension cells were then centrifuged, treated with red blood cell lysis solution (Promega, Cat#Z3141), and washed with autoclaved PBS. To quantify the satellite cell population, cells from both WT and *Prmt5*^{MKO} mice were stained with antibody cocktail consisting of CD31-PE (BioLegend, Cat#102408), CD45-PE (BioLegend, Cat#103106), Sca1-Pacific Blue (BioLegend, Cat#108120), and VCAM-APC (BioLegend, Cat#105718) for 30 min at 4°C in the dark. Satellite cells were identified and purified by gating with $CD31^{-}CD45^{-}Sca1^{-}VCAM1^{+}$ using a BD-FACS Aria III FACS system (BD Biosciences). For the quantification of immune cell population, CD45(Invitrogen, Cat#12-0451-82), CD11b (Invitrogen, Cat#25-0112-82), MHCII (Invitrogen, Cat#11-5322-82), and F4/80 (Invitrogen, Cat#11-5322-82) antibodies were used for analysis.

Immunoblotting analysis—Protein extraction from homogenized muscle tissues and primary myoblasts was carried out using RIPA buffer, which contained 25 mM Tris-HCl (pH 8.0), 150 mM NaCl, 1 mM EDTA, 0.5% NP-40, and 0.1% SDS), supplemented with proteinase inhibitor and phenylmethylsulphonyl fluoride (PMSF). The quantification of supernatant proteins was performed using Peirce BCA Protein Assay Reagent (Pierce Biotechnology). The proteins were separated by electrophoresis, and then transferred onto a polyvinylidene fluoride (PVDF) membrane. After blocking the membrane with 5% fat-free milk for 1 h at room temperature, primary antibodies were incubated with the membrane overnight at 4°C. Detection of immunoreactivity was performed using an enhanced chemiluminescence western blotting substrate (Santa Cruz Biotechnology) on a FluorChem R system (Proteinsimple). For Subcellular fractions, trypsinized cells were incubated in a hypotonic buffer (0.1% NP40, 20 mM Tris-HCL (pH 7.4), 10 mM KCL, 2 mM $MgCl_2$, 1 mM EGTA, 0.5 mM DTT, 5 mM PMSF) for 3 min and were subjected to centrifugation at 2,000 rpm. The resulting supernatant was further centrifuged at 15,000 rpm to separate and collect only supernatant (cytosolic fraction). Subsequently, the pellet was washed twice using isotonic buffer (0.1% NP40, 20 mM Tris-HCl (pH 7.4), 150 mM KCL, 2 mM $MgCl_2$, 1 mM EGTA, 0.5 mM DTT, 0.5 mM PMSF) for 3 min each. These washes

were performed to eliminate any cytosolic proteins, and the resultant pellt was designated as the nuclear fraction.[87]

Total RNA extraction and qRT-PCR—Cell and tissues were subjected to RNA extraction using TRIzol reagent (Thermo Fisher Scientific) according to the manufacturer's instruction. The extracted 2 mg of total RNA was reverse transcribed using random primers, M-MLV reverse transcriptase, and DTT. Real-time qPCR was performed using SYBR green master mix and gene-specific primers, listed in Table S1. Changes in relative expression of mRNA level were analyzed by employing the $2^{-\Delta\Delta CT}$ method and normalized to β-actin.

Sea horse—Primary myoblasts cells (1×10^5 cells) extracted from hindlimb muscles of WT and *Rosa*^{CreER}/*Prmt5*$^{f/f}$ mice were seeded into XF24 microplates (SeaHorse, Bioscience). On the day of the measurements, the primary myoblasts were thoroughly washed three times using XF medium (supplemented with SeaHorse XF RPMI medium, 5 mM glucose, 2 mM pyruvate, 1 mM glutamine, pH 7.4) and were then pre-incubated for 1 h at 37°C in a non-CO_2 incubator using the same medium. Subsequently, oligomycin (3 μM), FCCP (3 μM), Rotenone (1.5 μM), and Antimycin A (1.5 μM) were preloaded in a sequential manner into the cartridges, which were injected into XF wells to monitor oxygen consumption rate (OCR, pmol/min). The SeaHorse Wave software was used to measure the respiration rates of all mitochondria and normalize them based on the cellular protein contents.

Oil Red O (ORO) staining—Primary myoblasts were fixed with 4% PFA for 10 min, followed by staining with ORO working solution for 30 min at room temperature. After rinsing with PBs to remove excess stain, the ORO-stained myoblasts were imaged under bright field microscopy. Once imaging was completed, the cells were allowed to air dry for 1 h. The stained lipids were eluted from the myoblasts by adding isopropanol to each well and incubating for 20 min with gentle shaking. The eluted solution was transferred to a new microplate, and the absorbance was measured at a suitable wavelength (e.g., 510 nm) using a microplate reader.

Cell cycle assay—The myofibers from both WT and *Prmt5*^{MKO} mice were isolated and cultured in a Petri dish (60 mm) coated with horse serum in DMEM supplemented with 20% FBS (HyClone), 4 ng/ml basic FGF (Promega), and 1% Penicillin-streptomycin (HyClone) at 37°C. EdU (Cayman Chemical) was added to the culture medium at a concentration of 1mM. Cultured single myofibers were sampled at the designated time points for analysis.

QUANTIFICATION AND STATISTICAL ANALYSIS

A minimum of three biological replicates were utilized for performing experiments *in vivo*. The muscle histological analysis encompassing measurements including myofiber sectional area (CSA), the number of central nuclei, and myogenic cells per area were quantified using Fiji-imageJ software or Adobe PhotoShop software. The determination of the fusion index involved assessing the proportion of nuclei within MF20+ myotubes to the total nuclei number per image. The intensity of Bodipy in primary myoblasts was assessed using the Fiji-ImageJ software. The sample size or number of replicates (denoted as 'n') for each experiment is indicated in the figure legends. The data were presented as mean ± standard

error of the mean (S.E.M). All quantitative analyses were conducted using Student's t-test with a two-tail distribution, calculated using GraphPad Prism. The significance levels are denoted by $p < 0.05$, $p < 0.01$, $p < 0.001$, and $p < 0.0001$. A p value <0.05 was defined as statistically significant, whereas a p value greater than 0.05 was considered not significant.

Supplementary Material

Refer to Web version on PubMed Central for supplementary material.

ACKNOWLEDGMENTS

This work was supported by grants from the US National Institutes of Health (R01AR078695, R01DK132819, R01AR079235) to S.K. and (F31AR077424) to S.O. We thank Dr. Changdeng Hu (Purdue University, USA) for kindly providing the *Prmt5*$^{flox/flox}$ mice. We extend our gratitude to Jun Wu and Mary Larimore for their valuable contributions in maintaining the mouse colony and the members of the Kuang laboratory for their valuable insights and critical comments.

REFERENCES

1. Blau HM, Cosgrove BD, and Ho ATV((2015). The central role of muscle stem cells in regenerative failure with aging. Nat. Med. 21, 854–862. [PubMed: 26248268]
2. Yin H, Price F, and Rudnicki MA (2013). Satellite cells and the muscle stem cell niche. Physiol. Rev. 93, 23–67. [PubMed: 23303905]
3. Rodriguez-Outeiriño L, Hernandez-Torres F, Ramírez-de Acuña F, Matías-Valiente L, Sanchez-Fernandez C, Franco D, and Aranega AE (2021). Muscle satellite cell heterogeneity: does embryonic origin matter? Front. Cell Dev. Biol. 9, 750534. [PubMed: 34722534]
4. Relaix F, Bencze M, Borok MJ, Der Vartanian A, Gattazzo F, Mademtzoglou D, Perez-Diaz S, Prola A, Reyes-Fernandez PC, Rotini A, and Taglietti 5th.. (2021). Perspectives on skeletal muscle stem cells. Nat. Commun. 12, 692. [PubMed: 33514709]
5. Pallafacchina G, Blaauw B, and Schiaffino S (2013). Role of satellite cells in muscle growth and maintenance of muscle mass. Nutr. Metabol. Cardiovasc. Dis. 23, S12–S18.
6. Xia Q, Huang X, Huang J, Zheng Y, March ME, Li J, and Wei Y (2021). The role of autophagy in skeletal muscle diseases. Front. Physiol. 12, 638983. [PubMed: 33841177]
7. Yang W, Huang J, Wu H, Wang Y, Du Z, Ling Y, Wang W, Wu Q, and Gao W (2020). Molecular mechanisms of cancer cachexia-induced muscle atrophy. Mol. Med. Rep. 22, 4967–4980. [PubMed: 33174001]
8. Zhang S, Peng X, Yang S, Li X, Huang M, Wei S, Liu J, He G, Zheng H, Yang L, et al. (2022). The regulation, function, and role of lipophagy, a form of selective autophagy, in metabolic disorders. Cell Death Dis. 13, 132. [PubMed: 35136038]
9. Ho TT, Warr MR, Adelman ER, Lansinger OM, Flach J, Verovskaya EV, Figueroa ME, and Passegué E (2017). Autophagy maintains the metabolism and function of young and old stem cells. Nature 543, 205–210. [PubMed: 28241143]
10. Boya P, Codogno P, and Rodriguez-Muela N (2018). Autophagy in stem cells: repair, remodelling and metabolic reprogramming. Development 145, dev146506. [PubMed: 29483129]
11. Chang NC (2020). Autophagy and stem cells: self-eating for self-renewal. Front. Cell Dev. Biol. 8, 138. [PubMed: 32195258]
12. Tang AH, and Rando TA (2014). Induction of autophagy supports the bioenergetic demands of quiescent muscle stem cell activation. EMBO J. 33, 2782–2797. [PubMed: 25316028]
13. Fiacco E, Castagnetti F, Bianconi V, Madaro L, De Bardi M, Nazio F, D'Amico A, Bertini E, Cecconi F, Puri PL, and Latella L (2016). Autophagy regulates satellite cell ability to regenerate normal and dystrophic muscles. Cell Death Differ. 23, 1839–1849. [PubMed: 27447110]

14. Yue F, Oprescu SN, Qiu J, Gu L, Zhang L, Chen J, Narayanan N, Deng M, and Kuang S (2022). Lipid droplet dynamics regulate adult muscle stem cell fate. Cell Rep. 38, 110267. [PubMed: 35045287]
15. Lam T, Harmancey R, Vasquez H, Gilbert B, Patel N, Hariharan V, Lee A, Covey M, and Taegtmeyer H (2016). Reversal of intramyocellular lipid accumulation by lipophagy and a p62-mediated pathway. Cell Death Dis. 2, 16061–16112.
16. Yue F, Bi P, Wang C, Shan T, Nie Y, Ratliff TL, Gavin TP, and Kuang S (2017). Pten is necessary for the quiescence and maintenance of adult muscle stem cells. Nat. Commun. 8, 14328. [PubMed: 28094257]
17. Aman Y, Schmauck-Medina T, Hansen M, Morimoto RI, Simon AK, Bjedov I, Palikaras K, Simonsen A, Johansen T, Tavernarakis N, et al. (2021). Autophagy in healthy aging and disease. Nat. Aging 1, 634–650. [PubMed: 34901876]
18. Farhan M, Silva M, Li S, Yan F, Fang J, Peng T, Hu J, Tsao MS, Little P, and Zheng W (2020). The role of FOXOs and autophagy in cancer and metastasis—Implications in therapeutic development. Med. Res. Rev. 40, 2089–2113. [PubMed: 32474970]
19. Yue J, Aobulikasimu A, Sun W, Liu S, Xie W, and Sun W (2022). Targeted regulation of FoxO1 in chondrocytes prevents age-related osteoarthritis via autophagy mechanism. J. Cell Mol. Med. 26, 3075–3082. [PubMed: 35560791]
20. Zhao Y, Yang J, Liao W, Liu X, Zhang H, Wang S, Wang D, Feng J, Yu L, and Zhu W-G (2010). Cytosolic FoxO1 is essential for the induction of autophagy and tumour suppressor activity. Nat. Cell Biol. 12, 665–675. [PubMed: 20543840]
21. Wang B, Ding W, Zhang M, Li H, Guo H, Lin L, Chen J, and Gu Y (2016). Role of FOXO1 in aldosterone-induced autophagy: A compensatory protective mechanism related to podocyte injury. Oncotarget 7, 45331–45351. [PubMed: 27244896]
22. Wang S, Xia P, Huang G, Zhu P, Liu J, Ye B, Du Y, and Fan Z (2016). FoxO1-mediated autophagy is required for NK cell development and innate immunity. Nat. Commun. 7, 11023. [PubMed: 27010363]
23. Zhou J, Liao W, Yang J, Ma K, Li X, Wang Y, Wang D, Wang L, Zhang Y, Yin Y, et al. (2012). FOXO3 induces FOXO1-dependent autophagy by activating the AKT1 signaling pathway. Autophagy 8, 1712–1723. [PubMed: 22931788]
24. Kamei Y, Miura S, Suzuki M, Kai Y, Mizukami J, Taniguchi T, Mochida K, Hata T, Matsuda J, Aburatani H, et al. (2004). Skeletal Muscle FOXO1 (FKHR) Transgenic Mice Have Less Skeletal Muscle Mass, Down-regulated Type I (Slow Twitch/Red Muscle) Fiber Genes, and Impaired Glycemic Control*[boxs]. J. Biol. Chem. 279, 41114–41123. [PubMed: 15272020]
25. Xu M, Chen X, Chen D, Yu B, and Huang Z (2017). FoxO1: a novel insight into its molecular mechanisms in the regulation of skeletal muscle differentiation and fiber type specification. Oncotarget 8, 10662–10674. [PubMed: 27793012]
26. Leduc-Gaudet J-P, Franco-Romero A, Cefis M, Moamer A, Broering FE, Milan G, Sartori R, Chaffer TJ, Dulac M, Marcangeli V, et al. (2023). MYTHO is a novel regulator of skeletal muscle autophagy and integrity. Nat. Commun. 14, 1199. [PubMed: 36864049]
27. So H-K, Kim S, Kang J-S, and Lee S-J (2021). Role of protein arginine methyltransferases and inflammation in muscle pathophysiology. Front. Physiol. 12, 712389. [PubMed: 34489731]
28. Stouth DW, VanLieshout TL, Shen NY, and Ljubicic V (2017). Regulation of skeletal muscle plasticity by protein arginine methyltransferases and their potential roles in neuromuscular disorders. Front. Physiol. 8, 870. [PubMed: 29163212]
29. Blanc RS, Vogel G, Li X, Yu Z, Li S, and Richard S (2017). Arginine methylation by PRMT1 regulates muscle stem cell fate. Mol. Cell Biol. 37, e00457–16. [PubMed: 27849571]
30. Kawabe YI, Wang YX, McKinnell IW, Bedford MT, and Rudnicki MA (2012). Carm1 regulates Pax7 transcriptional activity through MLL1/2 recruitment during asymmetric satellite stem cell divisions. Cell Stem Cell 11, 333–345. [PubMed: 22863532]
31. Blanc RS, Vogel G, Chen T, Crist C, and Richard S (2016). PRMT7 preserves satellite cell regenerative capacity. Cell Rep. 14, 1528–1539. [PubMed: 26854227]

32. Jeong H-J, Lee S-J, Lee H-J, Kim H-B, Anh Vuong T, Cho H, Bae G-U, and Kang J-S (2020). Prmt7 promotes myoblast differentiation via methylation of p38MAPK on arginine residue 70. Cell Death Differ. 27, 573–586. [PubMed: 31243342]
33. Zhang T, Gu€nther S, Looso M, Künne C, Krüger M, Kim J, Zhou Y, and Braun T (2015). Prmt5 is a regulator of muscle stem cell expansion in adult mice. Nat. Commun. 6, 7140. [PubMed: 26028225]
34. Jia Z, Yue F, Chen X, Narayanan N, Qiu J, Syed SA, Imbalzano AN, Deng M, Yu P, Hu C, and Kuang S (2020). Protein arginine methyltransferase PRMT5 regulates fatty acid metabolism and lipid droplet biogenesis in white adipose tissues. Adv. Sci. 7, 2002602.
35. Chargé SBP, and Rudnicki MA (2004). Cellular and molecular regulation of muscle regeneration. Physiol. Rev. 84, 209–238. [PubMed: 14715915]
36. Kim KH, Jia Z, Snyder M, Chen J, Qiu J, Oprescu SN, Chen X, Syed SA, Yue F, Roseguini BT, et al. (2023). PRMT5 links lipid metabolism to contractile function of skeletal muscles. EMBO Rep. 24, e57306. [PubMed: 37334900]
37. Singh R, Kaushik S, Wang Y, Xiang Y, Novak I, Komatsu M, Tanaka K, Cuervo AM, and Czaja MJ (2009). Autophagy regulates lipid metabolism. Nature 458, 1131–1135. [PubMed: 19339967]
38. Yamagata K, Daitoku H, Takahashi Y, Namiki K, Hisatake K, Kako K, Mukai H, Kasuya Y, and Fukamizu A (2008). Arginine methylation of FOXO transcription factors inhibits their phosphorylation by Akt. Mol. Cell 32, 221–231. [PubMed: 18951090]
39. Bik E, Mateuszuk L, Orleanska J, Baranska M, Chlopicki S, and Majzner K (2021). Chloroquine-induced accumulation of autophagosomes and lipids in the endothelium. Int. J. Mol. Sci. 22, 2401. [PubMed: 33673688]
40. Kim K, Orvis J, and Stolfi A (2022). Pax3/7 regulates neural tube closure and patterning in a non-vertebrate chordate. Front. Cell Dev. Biol. 10, 999511. [PubMed: 36172287]
41. Jostes B, Walther C, and Gruss P (1990). The murine paired box gene, Pax7, is expressed specifically during the development of the nervous and muscular system. Mech. Dev. 33, 27–37. [PubMed: 1982921]
42. Chittka A, Nitarska J, Grazini U, and Richardson WD (2012). Transcription factor positive regulatory domain 4 (PRDM4) recruits protein arginine methyltransferase 5 (PRMT5) to mediate histone arginine methylation and control neural stem cell proliferation and differentiation. J. Biol. Chem. 287, 42995–43006. [PubMed: 23048031]
43. Calabretta S, Vogel G, Yu Z, Choquet K, Darbelli L, Nicholson TB, Kleinman CL, and Richard S (2018). Loss of PRMT5 promotes PDGFRα degradation during oligodendrocyte differentiation and myelination. Dev. Cell 46, 426–440.e5. [PubMed: 30057274]
44. Bezzi M, Teo SX, Muller J, Mok WC, Sahu SK, Vardy LA, Bonday ZQ, and Guccione E (2013). Regulation of constitutive and alternative splicing by PRMT5 reveals a role for Mdm4 pre-mRNA in sensing defects in the spliceosomal machinery. Genes Dev. 27, 1903–1916. [PubMed: 24013503]
45. Relaix F, Rocancourt D, Mansouri A, and Buckingham M (2004). Divergent functions of murine Pax3 and Pax7 in limb muscle development. Genes Dev. 18, 1088–1105. [PubMed: 15132998]
46. Messina G, and Cossu G (2009). The origin of embryonic and fetal myoblasts: a role of Pax3 and Pax7. Genes Dev. 23, 902–905. [PubMed: 19390084]
47. Buckingham M, and Relaix F (2007). The role of Pax genes in the development of tissues and organs: Pax3 and Pax7 regulate muscle progenitor cell functions. Annu. Rev. Cell Dev. Biol. 23, 645–673. [PubMed: 17506689]
48. Hutcheson DA, Zhao J, Merrell A, Haldar M, and Kardon G (2009). Embryonic and fetal limb myogenic cells are derived from developmentally distinct progenitors and have different requirements for β-catenin. Genes Dev. 23, 997–1013. [PubMed: 19346403]
49. Kuang S, Chargé SB, Seale P, Huh M, and Rudnicki MA (2006). Distinct roles for Pax7 and Pax3 in adult regenerative myogenesis. J. Cell Biol. 172, 103–113. [PubMed: 16391000]
50. Seale P, Sabourin LA, Girgis-Gabardo A, Mansouri A, Gruss P, and Rudnicki MA (2000). Pax7 is required for the specification of myogenic satellite cells. Cell 102, 777–786. [PubMed: 11030621]
51. Oustanina S, Hause G, and Braun T (2004). Pax7 directs postnatal renewal and propagation of myogenic satellite cells but not their specification. EMBO J. 23, 3430–3439. [PubMed: 15282552]

52. Dacwag CS, Ohkawa Y, Pal S, Sif S, and Imbalzano AN (2007). The protein arginine methyltransferase Prmt5 is required for myogenesis because it facilitates ATP-dependent chromatin remodeling. Mol. Cell Biol. 27, 384–394. [PubMed: 17043109]
53. Knobloch M, Braun SMG, Zurkirchen L, Von Schoultz C, Zamboni N, Araúzo-Bravo MJ, Kovacs WJ, Karalay Ö, Suter U, Machado RAC, et al. (2013). Metabolic control of adult neural stem cell activity by Fasn-dependent lipogenesis. Nature 493, 226–230. [PubMed: 23201681]
54. Ramosaj M, Madsen S, Maillard V, Scandella V, Sudria-Lopez D, Yuizumi N, Telley L, and Knobloch M (2021). Lipid droplet availability affects neural stem/progenitor cell metabolism and proliferation. Nat. Commun. 12, 7362. [PubMed: 34934077]
55. Zhu Q, Wang D, Liang F, Tong X, Liang Z, Wang X, Chen Y, and Mo D (2022). Protein arginine methyltransferase PRMT1 promotes adipogenesis by modulating transcription factors C/EBPb and PPARg. J. Biol. Chem. 298, 102309. [PubMed: 35921899]
56. Lei Y, Han P, Chen Y, Wang H, Wang S, Wang M, Liu J, Yan W, Tian D, and Liu M (2022). Protein arginine methyltransferase 3 promotes glycolysis and hepatocellular carcinoma growth by enhancing arginine methylation of lactate dehydrogenase A. Clin. Transl. Med. 12, e686. [PubMed: 35090076]
57. Soleimani VD, and Rudnicki MA (2011). New insights into the origin and the genetic basis of rhabdomyosarcomas. Cancer Cell 19, 157–159. [PubMed: 21316595]
58. Boscolo Sesillo F, Fox D, and Sacco A (2019). Muscle stem cells give rise to rhabdomyosarcomas in a severe mouse model of Duchenne muscular dystrophy. Cell Rep. 26, 689–701.e6. [PubMed: 30650360]
59. Lee DE, Bareja A, Bartlett DB, and White JP (2019). Autophagy as a therapeutic target to enhance aged muscle regeneration. Cells 8, 183. [PubMed: 30791569]
60. Civiletto G, Dogan SA, Cerutti R, Fagiolari G, Moggio M, Lamperti C, Benincá C, Viscomi C, and Zeviani M (2018). Rapamycin rescues mitochondrial myopathy via coordinated activation of autophagy and lysosomal biogenesis. EMBO Mol. Med. 10, e8799.
61. Masiero E, and Sandri M (2010). Autophagy inhibition induces atrophy and myopathy in adult skeletal muscles. Autophagy 6, 307–309. [PubMed: 20104028]
62. Zhang K, Zhang Y, Gu L, Lan M, Liu C, Wang M, Su Y, Ge M, Wang T, Yu Y, et al. (2018). Islr regulates canonical Wnt signaling-mediated skeletal muscle regeneration by stabilizing Dishevelled-2 and preventing autophagy. Nat. Commun. 9, 5129. [PubMed: 30510196]
63. Carmignac V, Svensson M, Körner Z, Elowsson L, Matsumura C, Gawlik KI, Allamand V, and Durbeej M (2011). Autophagy is increased in laminin α2 chain-deficient muscle and its inhibition improves muscle morphology in a mouse model of MDC1A. Hum. Mol. Genet. 20, 4891–4902. [PubMed: 21920942]
64. Fu X, Wang H, and Hu P (2015). Stem cell activation in skeletal muscle regeneration. Cell. Mol. Life Sci. 72, 1663–1677. [PubMed: 25572293]
65. Van de Vyver M, and Myburgh KH (2012). Cytokine and satellite cell responses to muscle damage: interpretation and possible confounding factors in human studies. J. Muscle Res. Cell Motil. 33, 177–185. [PubMed: 22673937]
66. Lettieri Barbato D, Tatulli G, Aquilano K, and Ciriolo MR (2013). FoxO1 controls lysosomal acid lipase in adipocytes: implication of lipophagy during nutrient restriction and metformin treatment. Cell Death Dis. 4, e861. [PubMed: 24136225]
67. Xiong X, Tao R, DePinho RA, and Dong XC (2012). The autophagy-related gene 14 (Atg14) is regulated by forkhead box O transcription factors and circadian rhythms and plays a critical role in hepatic autophagy and lipid metabolism. J. Biol. Chem. 287, 39107–39114. [PubMed: 22992773]
68. van der Horst A, and Burgering BMT (2007). Stressing the role of FoxO proteins in lifespan and disease. Nat. Rev. Mol. Cell Biol. 8, 440–450. [PubMed: 17522590]
69. Pan CW, Jin X, Zhao Y, Pan Y, Yang J, Karnes RJ, Zhang J, Wang L, and Huang H (2017). AKT-phosphorylated FOXO 1 suppresses ERK activation and chemoresistance by disrupting IQGAP 1-MAPK interaction. EMBO J. 36, 995–1010. [PubMed: 28279977]
70. Du Y-N, Tang X-F, Xu L, Chen W-D, Gao P-J, and Han W-Q (2018). SGK1-FoxO1 signaling pathway mediates Th17/Treg imbalance and target organ inflammation in angiotensin II-induced hypertension. Front. Physiol. 9, 1581. [PubMed: 30524295]

71. Schachter TN, Shen T, Liu Y, and Schneider MF (2012). Kinetics of nuclear-cytoplasmic translocation of Foxo1 and Foxo3A in adult skeletal muscle fibers. Am. J. Physiol. Cell Physiol. 303, C977–C990. [PubMed: 22932683]
72. Yan L, Lavin VA, Moser LR, Cui Q, Kanies C, and Yang E (2008). PP2A regulates the pro-apoptotic activity of FOXO1. J. Biol. Chem. 283, 7411–7420. [PubMed: 18211894]
73. Chae Y-C, Kim J-Y, Park JW, Kim K-B, Oh H, Lee K-H, and Seo S-B (2019). FOXO1 degradation via G9a-mediated methylation promotes cell proliferation in colon cancer. Nucleic Acids Res. 47, 1692–1705. [PubMed: 30535125]
74. Sebastián D, and Zorzano A (2020). Self-eating for muscle fitness: autophagy in the control of energy metabolism. Dev. Cell 54, 268–281. [PubMed: 32693059]
75. Zhang X, Evans TD, Jeong S-J, and Razani B (2018). Classical and alternative roles for autophagy in lipid metabolism. Curr. Opin. Lipidol. 29, 203–211. [PubMed: 29601311]
76. Chakrabarti P, English T, Karki S, Qiang L, Tao R, Kim J, Luo Z, Farmer SR, and Kandror KV((2011). SIRT1 controls lipolysis in adipocytes via FOXO1-mediated expression of ATGL. J. Lipid Res. 52, 1693–1701. [PubMed: 21743036]
77. Gies V, Bekaddour N, Dieudonné Y, Guffroy A, Frenger Q, Gros F, Rodero MP, Herbeuval JP, and Korganow AS (2020). Beyond Antiviral Effects of Chloroquine/Hydroxychloroquine. Front Immunol 11, 1409. [PubMed: 32714335]
78. Devarajan A, and Vaseghi M (2021). Hydroxychloroquine can potentially interfere with immune function in COVID-19 patients: Mechanisms and insights. Redox Biol 38, 101810. [PubMed: 33360293]
79. Ziemkiewicz N, Hilliard G, Pullen NA, and Garg K (2021). The Role of Innate and Adaptive Immune Cells in Skeletal Muscle Regeneration. Int J Mol Sci 22, 3265. [PubMed: 33806895]
80. Naddaf E, Paul P, and AbouEzzeddine OF (2021). Chloroquine and Hydroxychloroquine Myopathy: Clinical Spectrum and Treatment Outcomes. Front Neurol 11, 616075. [PubMed: 33603707]
81. Biguetti CC, Santiago JF Jr., Fiedler MW, Marrelli MT, and Brotto M (2021). The toxic effects of chloroquine and hydroxychloroquine on skeletal muscle: a systematic review and meta-analysis. Sci Rep 11, 6589. [PubMed: 33758324]
82. Kim KH, Jia Z, Snyder M, Chen J, Qiu J, Oprescu SN, Chen X, Syed SA, Yue F, Roseguini BT, Imbalzano AN, Hu C, and Kuang S (2023). PRMT5 links lipid metabolism to contractile function of skeletal muscles. EMBO Rep 24, e57306. [PubMed: 37334900]
83. Li Y, Cho MH, Lee SS, Lee DE, Cheong H, and Choi Y (2020). Hydroxychloroquine-loaded hollow mesoporous silica nanoparticles for enhanced autophagy inhibition and radiation therapy. J Control Release 325, 100–110. [PubMed: 32621826]
84. Huang D, Yue F, Qiu J, Deng M, and Kuang S (2020). Polymeric nanoparticles functionalized with muscle-homing peptides for targeted delivery of phosphatase and tensin homolog inhibitor to skeletal muscle. Acta Biomater 118, 196–206. [PubMed: 33053428]
85. Kim KH, Qiu J, and Kuang S (2020). Isolation, Culture, and Differentiation of Primary Myoblasts Derived from Muscle Satellite Cells. Bio. Protoc. 10, e3686.
86. Liu L, Cheung TH, Charville GW, and Rando TA (2015). Isolation of skeletal muscle stem cells by fluorescence-activated cell sorting. Nat. Protoc. 10, 1612–1624. [PubMed: 26401916]
87. Senichkin VV, Prokhorova EA, Zhivotovsky B, and Kopeina GS (2021). Simple and efficient protocol for subcellular fractionation of normal and apoptotic cells. Cells 10, 852. [PubMed: 33918601]

Highlights

- PRMT5 is essential for muscle development and function *in vivo*
- PRMT5 regulates fate of muscle stem cells and muscle regenerative capacity
- PRMT5 governs autophagy through FoxO1 methylation, influencing its subcellular localization
- Autophagy inhibition partially improves muscle regeneration in *Prmt5* KO mice

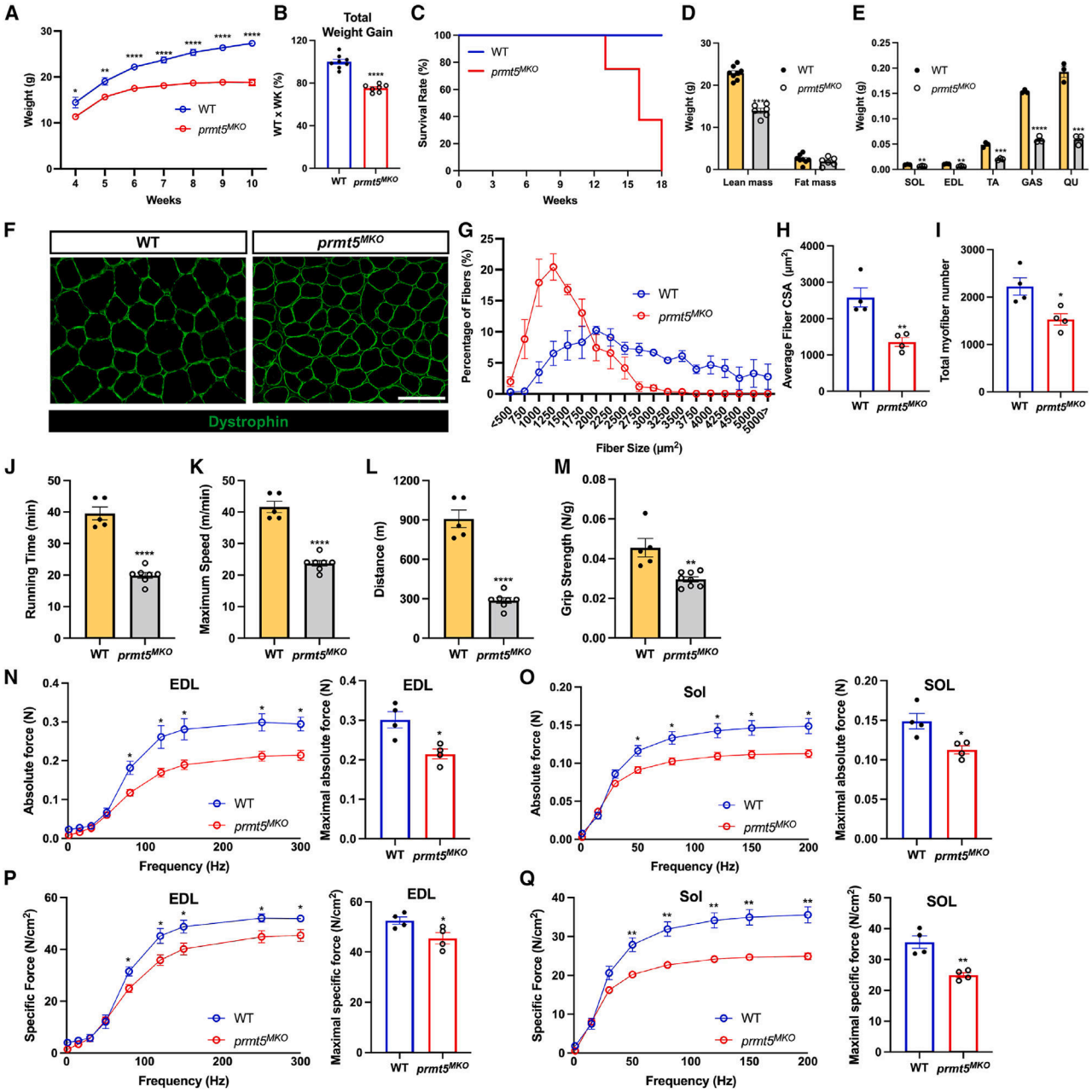

Figure 1. Conditional KO of *Prmt5* in embryonic myoblasts (*Prmt5*^{MKO}) reduces muscle mass, impairs muscle function, and leads to pre-term death in adult mice

(A and B) Growth curve (A) and total body weight gain over 6 weeks (B) in 4-week-old WT and *Prmt5*^{MKO} mice (n = 7/group).

(C) Survival of adult WT and *Prmt5*^{MKO} mice; all KO mice died before reaching 18 weeks old (n = 15).

(D) Lean and fat mass of 8-week-old WT and *Prmt5*^{MKO} mice (n = 6) measured by EchoMRI body composition analyzer.

(E) Weight of *soleus* (SOL), *extensor digitorum longus* (EDL), *tibialis anterior* (TA), *gastrocnemius* (GAS), and *quadriceps* (QU) muscles in adult WT and *Prmt5*^{MKO} mice (n = 3).

(F) Myofiber morphology outlined by sarcolemma dystrophin immunofluorescence of TA muscle sections from WT and *Prmt5*^{MKO} mice (n = 4). Scale bar, 100 μm.

(G) Frequency distribution of TA muscle myofiber cross-sectional area (CSA) in adult WT and *Prmt5*^{MKO} mice (n = 4).

(H and I) Average myofiber CSA (H) and total myofiber number (I) per TA muscle of WT and *Prmt5*^{MKO} mice (n = 4).

(J–L) Running time (J), maximum speed (K), and running distance (L) of adult WT and *Prmt5*^{MKO} mice measured by treadmill exhaustion test (n = 5–7).

(M) Grip strength test normalized to body weight in adult WT and *Prmt5*^{MKO} mice (n = 5–8).

(N and O) Absolute contractile force as a function of frequency of electric stimulation (left) and maximal absolute force (right) measured in the EDL (N) and SOL (O) muscles isolated from adult WT and *Prmt5*^{MKO} mice (n = 4).

(P and Q) Specific force as a function of frequency (left) and maximal specific force (right) of EDL (P) and SOL (Q) muscles isolated from adult WT and *Prmt5*^{MKO} mice (n = 4).

Values are expressed as mean ± SEM. *p < 0.05, **p < 0.01, ***p < 0.001, ****p < 0.0001 by t tests. See also Figure S1.

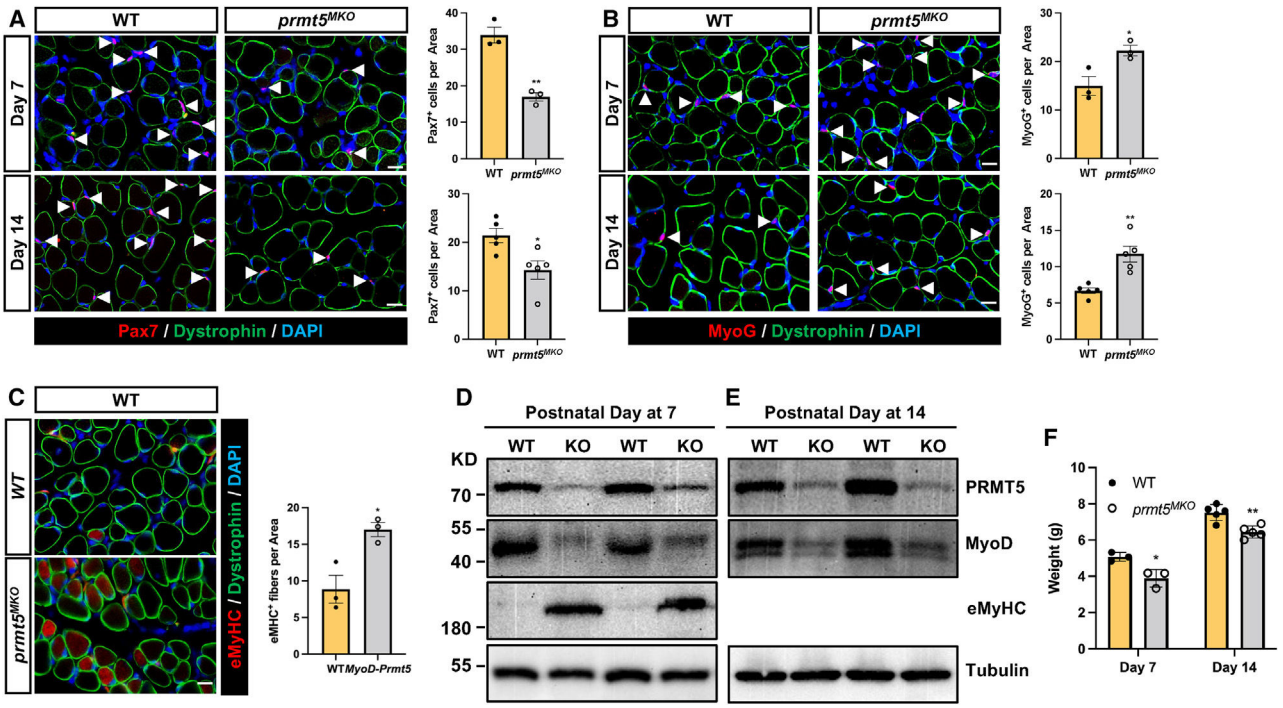

Figure 2. Prmt5 KO in embryonic myoblasts (*Prmt5*^{MKO}) delay postnatal myogenesis and muscle growth

(A and B) immunofluorescence of Pax7 (A) and MyoG (B) in the left panels and corresponding quantification of cells, in right panels, of WT and *Prmt5*^{MKO} TA muscle sections at P7 (n = 3) and P14 (n = 5). Myofiber membranes are stained with dystrophin and nuclei are stained by DAPI sarcolemma. Scale bar, 10 μm.

(C) eMyHC immunofluorescence (left) and quantification of eMyHC^{+} myofibers (right) in TA muscle of WT and *Prmt5*^{MKO} mice at P7 (n = 4–5). Scale bar, 10 μm.

(D and E) immunoblotting analysis showing the protein contents of PRMT5, MyoD, eMyHC, and tubulin at P7 (D) and P14 (E) in skeletal muscles of WT and *Prmt5*^{MKO} mice. KD, kilodalton size marker.

(F) Body weights of P7 and P14 WT and *Prmt5*^{MKO} mice (P7, n = 3; P14, n = 5).

Values are expressed as mean ± SEM. *p < 0.05, **p < 0.01 by t test. See also Figure S3.

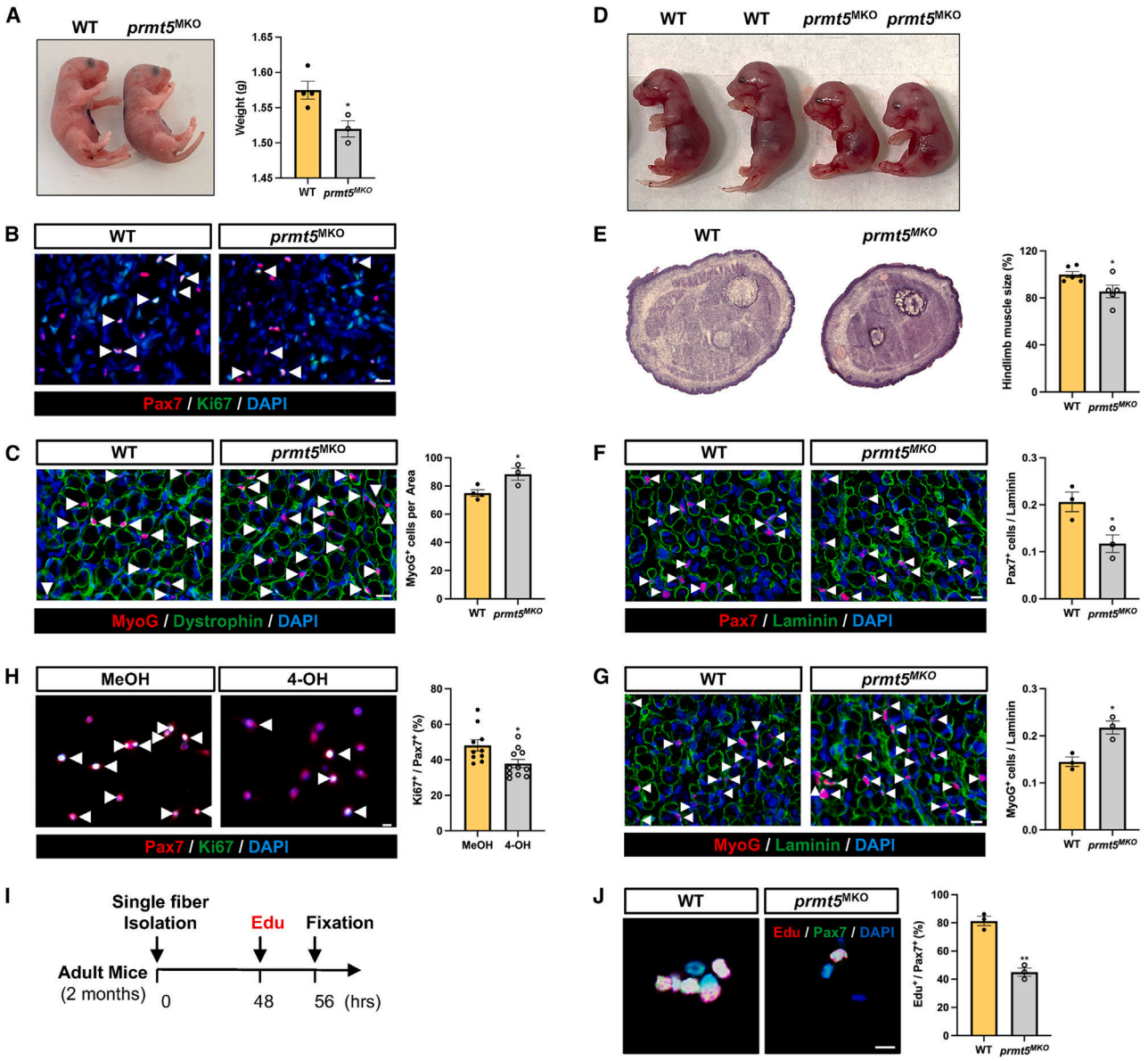

Figure 3. Prmt5 KO in embryonic myoblast (*Prmt5*^{MKO}) impedes cell proliferation and promotes premature differentiation, hampering embryonic and fetal myogenesis

(A) Gross morphology (left) and body weight (right) of newborn mice (P1) in WT and *Prmt5*^{MKO} mice (n = 3–4).

(B) Pax7^{+} and Ki67^{+} immunofluorescence (left) and quantification (right) in hindlimb cross sections of newborn WT and *Prmt5*^{MKO} mice (n = 3–4). Scale bar, 10 μm.

(C) MyoG immunofluorescence (left) and quantification of MyoG^{+} cells per area (right) in hindlimb muscle sections of P1 WT and *Prmt5*^{MKO} mice (n = 3–4). Scale bar, 10 μm.

(D) Gross morphology of E18.5 WT and *Prmt5*^{MKO} embryos.

(E) H&E staining (left) and quantification of E18.5 hindlimb (right) of WT and *Prmt5*^{MKO} mice.

(F and G) Pax7 (F) and MyoG (G) immunofluorescence images (left) and corresponding quantification of positive cells per myofiber (right) in WT and *Prmt5*^{MKO} E18.5 hindlimb sections (n = 3). Scale bar, 10 μm.

(H) Pax7 and Ki67 immunofluorescence (left) and percentage of proliferating (Ki67^{+}) cells among Pax7^{+} myoblasts (right). Primary myoblasts were treated with vehicle or 4-OH-TMX (4-hydroxyl-tamoxifen) (to induce deletion of Prmt5). Scale bar, 10 μm.

(I) Schematic outline of EdU incorporation assay to assess proliferating SCs on single myofibers isolated from adult WT and *Prmt5*^{MKO} mice.

(J) Pax7 immunofluorescence cells and EdU click labeling (left), along with the quantification (percentages of EdU^{+} cells among Pax7^{+} cells) grown on WT and *Prmt5*^{MKO} myofibers (right) (n = 3). Scale bar, 10 μm.

Values are expressed as mean ± SEM. *p < 0.05, **p < 0.01 by t test. See also Figure S2.

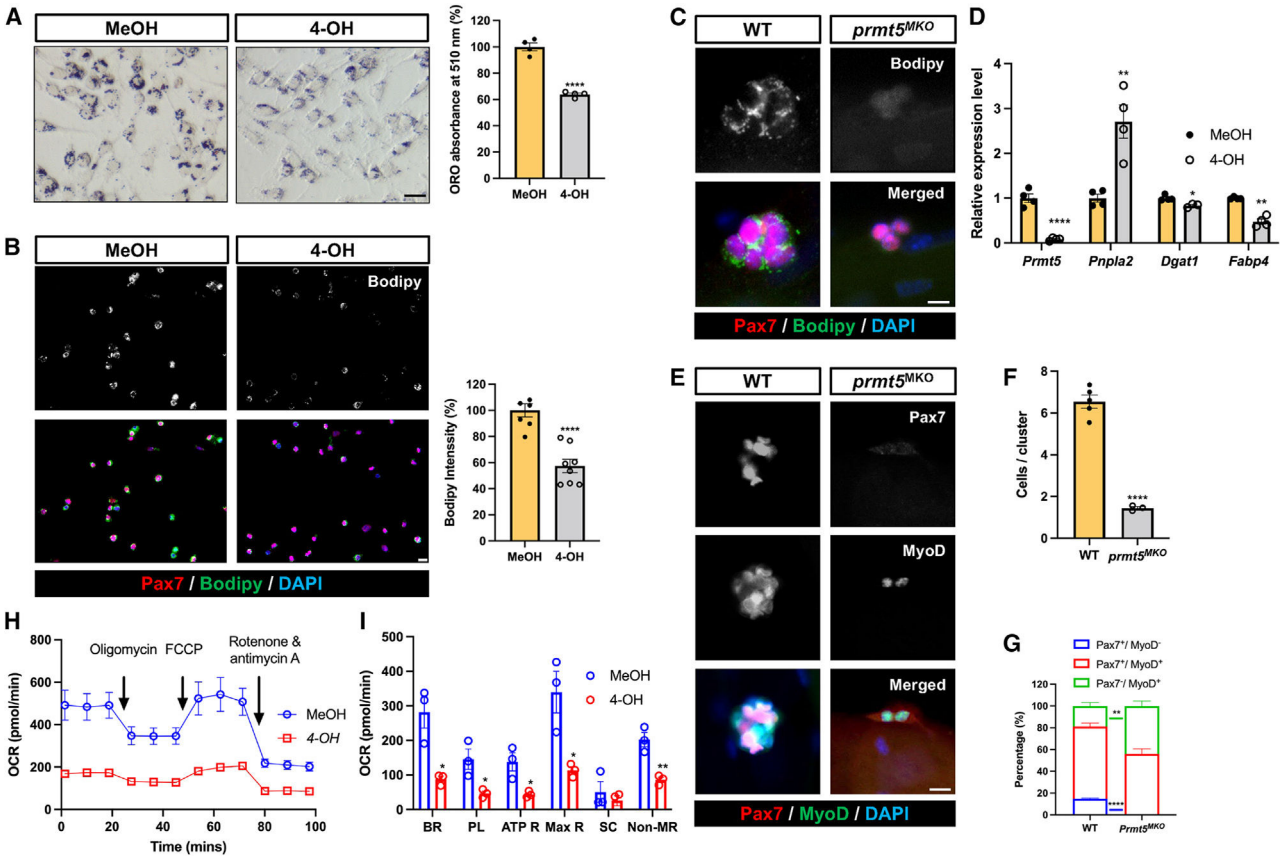

Figure 4. *Prmt5* KO diminishes LD abundance and oxidative respiration of SCs, disrupting their cell fate homeostasis

(A) Oil red O staining (left) and quantification (right) of LD content in control (MeOH) and Prmt5 KO (4-OH) myoblasts. Scale bar, 50 μm.

(B) Pax7 and Bodipy immunofluorescence (left) and quantification of Bodipy intensity (right) in control (MeOH) and *Prmt5* KO (4-OH) myoblasts. Scale bar, 10 mm.

(C) Pax7 and Bodipy immunofluorescence (left) and quantification of Bodipy intensity (right) in SCs after proliferating for 72 h on cultured single myofibers isolated from WT and $Prmt5^{MKO}$ mice. Scale bar, 10 μm.

(D) qPCR analysis of lipogenic marker (*Pnpla2*) and adipogenesis markers (*Dgat1, Fabp4*) in control (MeOH) and *Prmt5* KO (4-OH) myoblasts (n = 4).

(E–G) Pax7 and MyoD fluorescence to distinguish cell fate status in WT and $Prmt5^{MKO}$ SCs (E), quantification of SCs per cluster (F), and proportions of self-renewing ($Pax7^{+}MyoD^{-}$), proliferating ($Pax7^{+}MyoD^{+}$), and differentiating ($Pax7^{-}MyoD^{+}$) cells (G) after culturing on single myofibers for 72 h (n = 3). Scale bar, 10 μm.

(H) Seahorse measurement of oxygen consumption rate (OCR) in control (MeOH) and *Prmt5* KO (4-OH) myoblasts in response to sequential addition of oligomycin, carbonyl cyanide-p-trifluoromethoxyphenylhydrazone (FCCP), and rotenone/antimycin A (n = 3).

(I) Average OCR for basal respiration (BR), proton leak (PL), ATP respiration (ATP R), maximal respiration (Max R), spare capacity, and non-mitochondrial respiration (NR) based on H (n = 3). SC, spare capacity.

Values are expressed as mean ± SEM. *p < 0.05, **p < 0.01, ****p < 0.0001 by t test. See also Figure S4.

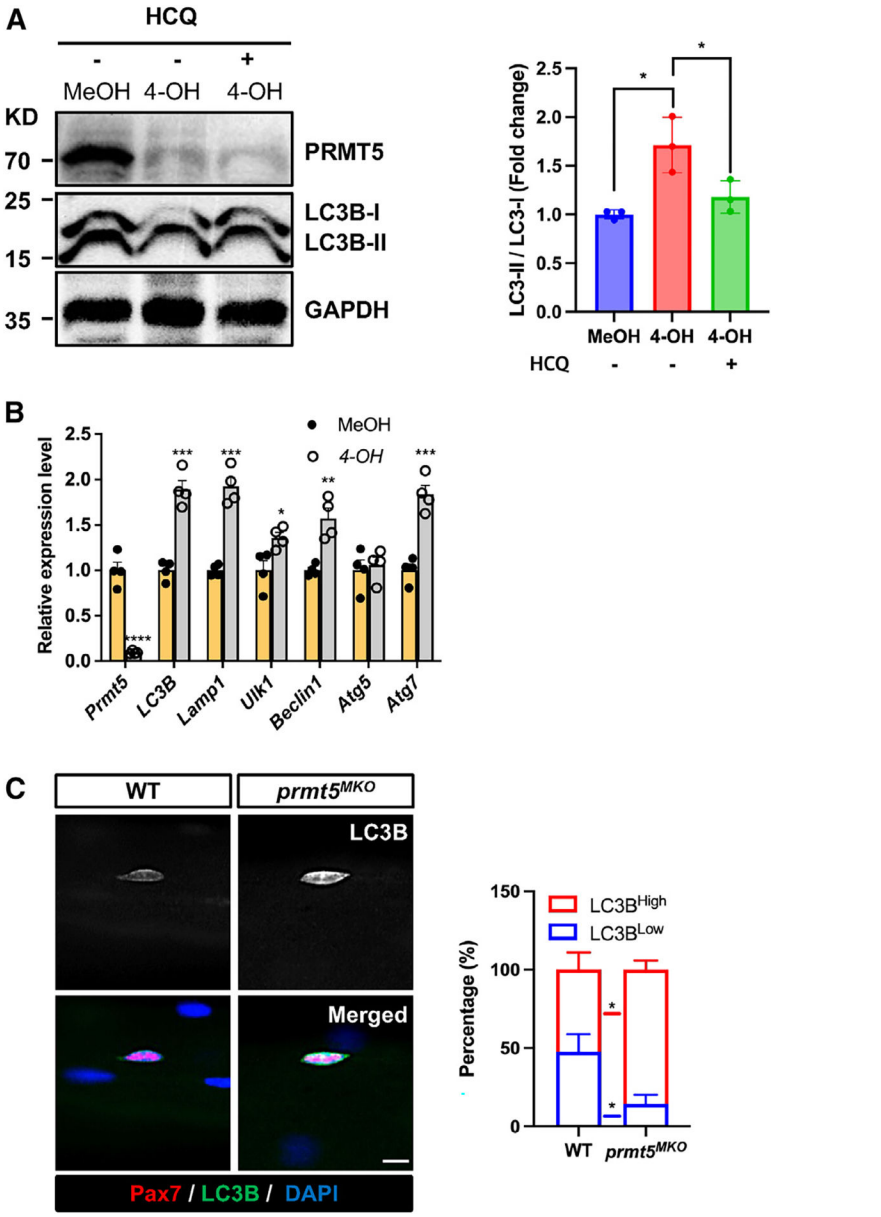

Figure 5. Prmt5 KO activates autophagy in satellite cells

(A) Western blotting showing levels of PRMT5, LC3B, and GAPDH in control (MeOH) and *Prmt5* KO (4-OH) myoblasts in the absence or presence of hydroxychloroquine (HCQ), along with quantified levels (normalized to GAPDH) of LC-II/I, as an indicator of autophagy (right). KD, kilodalton size marker.

(B) qPCR analysis of autophagy makers in control (MeOH) and *Prmt5* KO (4-OH) myoblasts (n = 4).

(C) Pax7 and LC3B immunofluorescence (left) and the relative intensity of LC3B (right) in Pax7^{+} cells grown on freshly isolated single myofibers from WT and *Prmt5*^{MKO} mice (n = 4). Scale bar, 10 μm.

Values are expressed as mean ± SEM. *p < 0.05, **p < 0.01, ***p < 0.001, ****p < 0.0001 by t test. See also Figure S5.

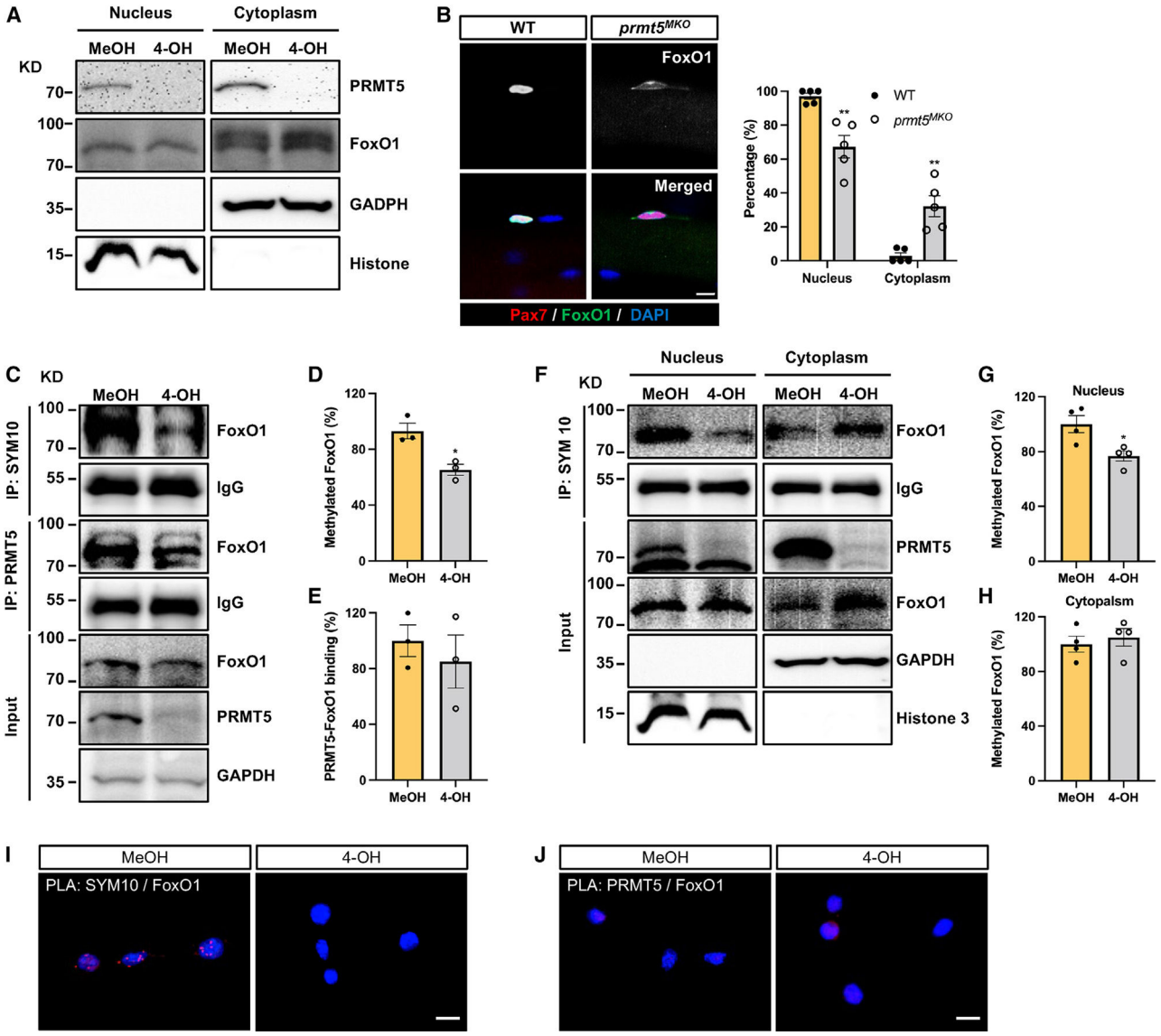

Figure 6. PRMT5 mediates methylation of FoxO1 to alter its subcellular localization

(A) Western blot images showing subcellular fraction of control (MeOH) and *Prmt5* KO (4-OH) myoblasts and cytoplasmic retention of FoxO1 in *Prmt5* KO cells. KD, kilodalton size marker.

(B) Pax7 and FoxO1 immunofluorescence (left) of SCs on freshly isolated myofibers from WT and *Prmt5*^{MKO} mice, along with quantification of FoxO1 subcellular location (right) (n = 5). Scale bar, 10 μm.

(C) Control (MeOH) and *Prmt5* KO (4-OH) myoblasts were immunoprecipitated with SYM10 and PRMT5 antibody and blotted with FoxO1, PRMT5, and GAPDH antibodies. KD, kilodalton size marker.

(D and E) Quantification of methylated FoxO1 (D) and PRMT5-FoxO1 binding (E) (n = 3).

(F) Control (MeOH) and *Prmt5* KO (4-OH) myoblasts were immunoprecipitated with SYM10 after subcellular fractionation and blotted with PRMT5, FoxO1, GAPDH, and histone 3 antibodies. KD, kilodalton size marker.

(G and H) Quantification of methylated FoxO1 in the nucleus (G) and cytoplasm (H) (n = 4). (I and J) Proximity ligation assay (PLA) on control (MeOH) and *Prmt5* KO (4-OH) myoblasts using SYM10 and FoxO1 (I), or PRMT5 and FoxO1 (J) antibody pairs. The presence of red punta indicates potential protein modification or interaction. Scale bar, 10 μm. Values are expressed as mean ± SEM. *p < 0.05, **p < 0.01 by t test. See also Figure S6.

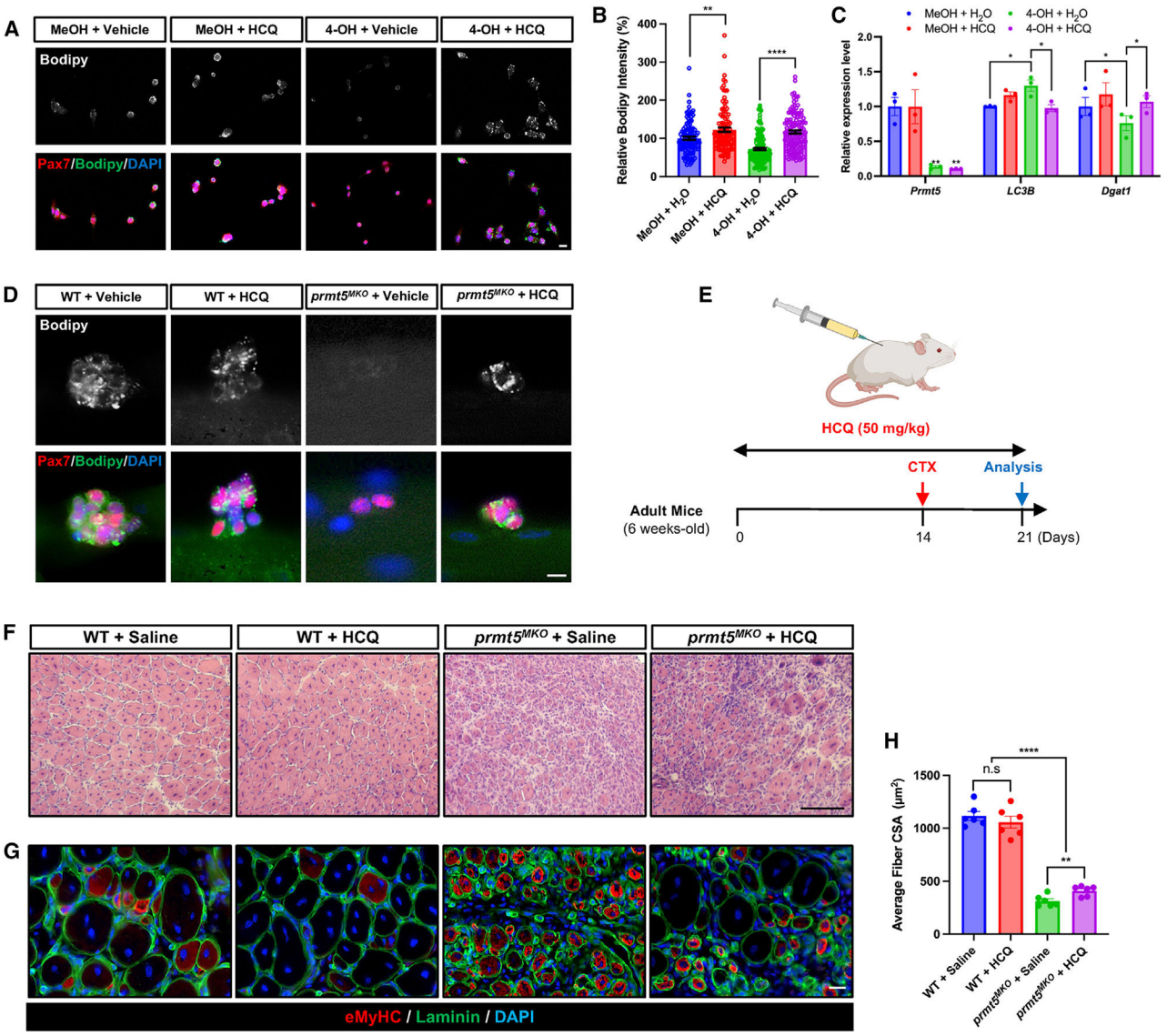

Figure 7. Pharmacological inhibition of autophagy alleviates defects of Prmt5-KO myoblasts

(A and B) Pax7 and Bodipy immunofluorescence (A), along with quantification of Bodipy intensity (B) in control (MeOH) and *Prmt5* KO (4-OH) myoblasts treated with or without HCQ. Scale bar, 10 μm.

(C) qPCR analysis of autophagy marker (*LC3B*) and lipid metabolism markers (*Dgat1*) in control (MeOH) and *Prmt5* KO (4-OH) myoblasts treated with or without HCQ (n = 3).

(D) Immunostaining of Pax7 and Bodipy in SCs after being cultured for 72 h on myofibers from WT and *Prmt5*^{MKO} treated with or without HCQ (n = 3). Scale bar, 10 μm.

(E) Experimental design for vehicle or HCQ treatment in adult WT and *Prmt5*^{MKO} mice to examine muscle regeneration.

(F) H&E images of WT and *Prmt5*^{MKO} TA muscle cross sections at 7 DPI after vehicle or HCQ treatment. Scale bar, 100 μm.

(G and H) Immunostaining of eMyHC and laminin (G) along with quantification of myofiber size (H) in WT and *Prmt5*^{MKO} TA muscle cross sections at 7 DPI after vehicle or HCQ treatment (n = 6). Scale bar, 10 μm.

Values are expressed as mean ± SEM. *p < 0.05, **p < 0.01, ***p < 0.001, ****p < 0.0001 by t test.

KEY RESOURCES TABLE

REAGENT or RESOURCE	SOURCE	IDENTIFIER
Antibodies		
Rabbit Polyclonal anti-PRMT5	Proteintech	Cat# 18436–1-AP, RRID: AB_2171798
Rabbit Polyclonal anti-Laminin	Sigma	Cat #L9393, RRID: AB_477163
Rabbit Polyclonal anti-Dystrophin	Abcam	Cat# ab15277, RRID: AB_301813
Rabbit Polyclonal anti-Tubulin	Abcam	Cat# ab6046, RRID: AB_2210370
Mouse Monoclonal anti-GAPDH	Santacruz	Cat# sc-32233, RRID: AB_627679
Rabbit Polyclonal anti-LC3B	Invitrogen	Ca# PA5–32254, RRID: AB_2549727
Mouse Monoclonal anti-FoxO1	Cell signaling	Cat# 14952, RRID: AB_2722487
Rabbit Polyclonal anti-FoxO1	Cell signaling	Cat# 2880, RRID: AB_2106495
Mouse Monoclonal anti-ATG7	Proteintech	Cat# 67341–1-Ig, RRID: AB_2882599
Rabbit Polyclonal anti-SYM10	Millipore	Cat# 07–412, RRID: AB_310594
Mouse Monoclonal anti-CD68	Abcam	Cat# Ab31630, RRID: AB_1141557
Mouse Monoclonal anti-Pax7	DSHB	Cat# Pax7, RRID: AB_2299243
Mouse Monoclonal anti-MyoD	Santa Cruz Biotechnology	Cat# sc-377460, RRID: AB_2813984
Mouse Monoclonal anti-MyoG	DSHB	Cat# F5D, RRID: AB_2146602
Mouse Monoclonal anti-MyHC	DSHB	Cat# MF20, RRID: AB_2147781
Mouse Monoclonal anti-eMyHC	DSHB	Cat# F1.652, RRID: AB_528358
Rabbit Polyclonal anti-Ki67	Abcam	Cat# ab15580, RRID: AB_443209
Mouse Monoclonal anti-Flag	Sigma	Cat# F1804, RRID: AB_262044
PE Rat anti-mouse CD31 antibody	BD Biosciences	Cat# 553373, RRID: AB_394819
PE anti-mouse CD45 antibody	eBioscience	Cat# 12–0451-82,RRID: AB_465668
Pacific Blue anti-mouse Ly-6A/E (Sca-1) antibody	BioLegned	Cat# 122520, RRID: AB_2143237
APC anti-mouse CD106 antibody	Biolegend	Cat# 105718, RRID: AB_1877141
PE-Cy7 anti-mouse CD11b	eBioscience	Cat# 25–0112-82, RRID: AB_469588
FITC anti-mouse MHC II	eBioscience	Cat# 11–5322-82, RRID: AB465235
FITC anti-mouse F4/80	eBioscience	Cat# 11–4801-81, RRID AB_2735037
Alexa 568 goat anti-mouse IgG1	Thermo Fisher Scientiic	Cat# A-21124, RRID: AB_2535766
Alexa 647 goat anti-mouse IgG2b	Thermo Fisher Scientiic	Cat# A-21242, RRID: AB_2535811
Alexa 488 goat-anti mouse IGM	Thermo Fisher Scientiic	Cat# A21042, RRID: AB_141357
Alexa 488 goat-anti rabbit IgG	Thermo Fisher Scientiic	Cat# A-11034, RRID: AB_2576217
HRP AffiniPure goat anti-mouse IgG	Jackson ImmunoResearch	Cat# 115–035-003, RRID: AB_10015289
HRP AffiniPure goat anti-rebbit IgG	Jackson ImmunoResearch	Cat# 111–035-003, RRID: AB_2313567
Chemicals, peptides, and recombinant proteins		
4-Hydroxytamoxifen (4-OHT)	Sigma-Aldrich	H6278
Hydroxychloroquine	Tcichemicals	H1306
Cardiotoxin	Sigma-Aldrich	217503
Collagenase, Type I	Worthington	LS004197
Collagenase, Type II	Worthington	LS004179

REAGENT or RESOURCE	SOURCE	IDENTIFIER
Dispase II	Sigma-Aldrich	04942078001
Red blood cell lysis solution	Promega	Z3141
Dulbecco's Modified Eagle Medium	Gibco	11995065
Ham's F10 Nutrient Mix	Gibco	11550043
Fetal bovine serum	HyClone	SH30080.03
Donor Hose Serum	Corning	MT35030CV
Opti-MEM	Gibco	31985070
Penicillin-Streptomycin	Sigma-Aldrich	P4333
Seahorse XF base medium	Agilent Technologies	103334–100
Phosphate-buffered saline	Gibco	21600–069
Bodipy 493/503	Invitrogen	D3922
M.O.M (Mouse on Mouse) blocking buffer	Vector lab	MKB-2213
DAPI	Invitrogen	D1306
O.C.T. Compound	Fisher Scientific	23–730-571
bFGF (Fibroblast growth factor, basic)	Promega	9PIG507
BD Matrigel Matrix	BD Science	356235
Collagen from rat tail	Sigma-Aldrich	C7661
5-Ethynyl-2'-deoxyuridine (EdU)	Cayman Chemical	20518
Lipofectamin 2000	Invitrogen	11668030
Xfect transection Reagent	Takara	631318
Goat serum	MP Biomedicals	08642921
TRIzol Reagent	Sigma-Aldrich	T9424
Chloroform	VWR Chemicals	BDH1109
Methanol	Fisher Scientific	A412–20
NP-40	Thermo Scientific	85124
SDS (Sodium Dodecyl Sulfrate)	Fisher Scientific	02–004-080
Ammonium acetate	Fisher Scientific	A637–500
PMSF	Calbiochem	7110-OP
Sodium pyruvate	Sigma-Aldrich	P5280
Paraformaldehyde	Sigma-Aldrich	P6148
Oil Red O (ORO)	Sigma-Aldrich	O0625
Sodium pyruvate	Sigma-Aldrich	P5280
Cycloheximide	Thermo Fisher Scientific	J66901–03
Critical commercial assays		
M-MLV reverse transcriptase	Invitrogen	28025021
Pierce BCA Protein Assay Reagent	Thermo Scientific	232225
Western Blotting Chemiluminescence Luminol Reagent	Santa Cruz Biotechnology	sc-2048
Seahorse XF Cell Mito Stress Test	Agilent Technologies	103015–100
Duolink *in situ* red Detection Reagent Red	Sigma	DUO92008
Experimental models: Cell lines		

REAGENT or RESOURCE	SOURCE	IDENTIFIER
Mouse: C2C12	ATCC	Cat# CRL-1772
Experimental models: Organisms/strains		
Mouse: FVB.Cg-*Myod1*$^{tm2.1(icre)Glh}$/J	The Jackson Laboratory	JAX Stock: #14140
Mouse: B6.129-*Gt(ROSA)26Sor*$^{tm1(cre/ERT2)Tyj}$/J	The Jackson Laboratory	JAX Stock: #008463
Mouse: *Prmt5*$^{flox/flox}$	Kim et al.[36], Jia et al.[34]	N/A
Oligonucleotides		
See Table S1	This paper	N/A
Recombinant DNA		
pcDNA3 Flag FKHR	Addgene	13507
1354 pcDNA3 flag FKHR ΔDB	Addgene	10694
1357 pcDNA3 flag FKHR AAA ΔDB	Addgene	10696
Software and algorithms		
FlowJo 10	FLOWJO, LLC	RRID: SCR_008520
Fiji-ImageJ		RRID:SCR_002285
Seahorse Wave	Agilent Technologies	RRID: SCR_014526
PRISM 6.0	GraphPad Prism	RRID:SCR_002798
Adobe Photoshop	Adobe Inc.	RRID: SCR_014199